AD NUMBER
ADB019116
LIMITATION CHANGES

TO:

Approved for public release; distribution is unlimited.

FROM:

Distribution authorized to U.S. Gov't. agencies only; Test and Evaluation; JUL 1976. Other requests shall be referred to Air Force Avionics Lab., Wright-Patterson AFB, OH 45433.
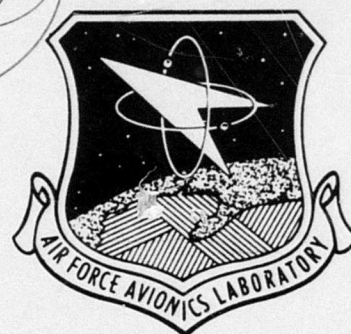
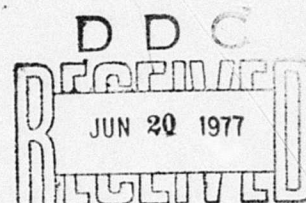| AUTHORITY |
|---|

AFSC/DOOS ltr 6 Aug 1991

AD B019116

GALLIUM PHOSPHIDE PHOTODIODE DEVELOPMENT

HONEYWELL RADIATION
2 FORBES ROAD
LEXINGTON, MA 02173

MARCH 1977

TECHNICAL REPORT AFAL-TR-76-146
FINAL REPORT FOR PERIOD OCTOBER 1974 - APRIL 1976

DDC

RECEIVED

JUN 20 1977

A

AD No.
DDC FILE COPY

AIR FORCE AVIONICS LABORATORY
AIR FORCE WRIGHT AERONAUTICAL LABORATORIES
AIR FORCE SYSTEMS COMMAND
WRIGHT-PATTERSON AIR FORCE BASE, OHIO 45433

This technical report has been reviewed and is approved for publication.

CHARLES T. ENNIS, Project Engineer
Electro-Optic Detectors Group
Electro-Optics Technology Branch

DONALD J. PEACOCK, Actg. Chief
Electro-Optic Detectors Group
Electro-Optics Technology Branch

FOR THE COMMANDER

WILLIAM C. SCHOONOVER, Chief
Electro-Optics Technology Branch
Electronic Technology Division

AIR FORCE - 20 APRIL 77 - 75

REPORT DOCUMENTATION PAGE		READ INSTRUCTIONS BEFORE COMPLETING FORM
1. REPORT NUMBER AFAL-TR-76-146	2. GOVT ACCESSION NO.	3. RECIPIENT'S CATALOG NUMBER
4. TITLE (and Subtitle) GALLIUM PHOSPHIDE PHOTODIODE DEVELOPMENT		5. TYPE OF REPORT & PERIOD COVERED Final Technical rept. October 1974-April 1976
		6. PERFORMING ORG. REPORT NUMBER
7. AUTHOR(s) A.M./Chiang R./Rotolante		8. CONTRACT OR GRANT NUMBER(s) F33615-75-C-1041
9. PERFORMING ORGANIZATION NAME AND ADDRESS Honeywell Radiation Center 2 Forbes Rd. Lexington, MA 02173		10. PROGRAM ELEMENT, PROJECT, TASK AREA & WORK UNIT NUMBERS 2001-03-39
11. CONTROLLING OFFICE NAME AND ADDRESS Air Force Avionics Laboratory Wright-Patterson Air Force Base Ohio 45433		12. REPORT DATE March 1977
		13. NUMBER OF PAGES 47
14. MONITORING AGENCY NAME & ADDRESS(if different from Controlling Office)		15. SECURITY CLASS. (of this report) UNCLASSIFIED
		15a. DECLASSIFICATION/DOWNGRADING SCHEDULE

16. DISTRIBUTION STATEMENT (of this Report)

Distribution limited to U.S. Government agencies only; report contains test and evaluation information, July 1976. Other requests for this document must be referred to AFAL/DHO-3, Wright-Patterson AFB, Ohio 45433.

17. DISTRIBUTION STATEMENT (of the abstract entered in Block 20, if different from Report)

18. SUPPLEMENTARY NOTES

19. KEY WORDS (Continue on reverse side if necessary and identify by block number)

Gallium Phosphide, Photodiode, Ion Implantation

20. ABSTRACT (Continue on reverse side if necessary and identify by block number)

The specific objectives of this program were to fabricate, test and deliver five single-element (detector size 0.01 x 0.01 inch^2) gallium phosphide (GaP) photovoltaic detectors with performance design goals (for each element) of $\eta > 30\%$ and NEP $\leq 2.5 \times 10^{-14}$ W/$\sqrt{\text{Hz}}$ at $\lambda = 0.4$ μm. These detectors demonstrate the feasibility for the eventual use of GaP

DD FORM 1473 EDITION OF 1 NOV 65 IS OBSOLETE
1 JAN 73

404486

photodiodes in a synchronous orbit, strapdown star sensor. Additionally, photoconductive test samples were fabricated in order to evaluate the characteristics of copper-doped GaP crystals. The work effort under this contract resulted in the production, test and delivery of five high performance Mg^{+} ion implanted GaP photovoltaic detectors. NEP as low as 1.6×10^{-14} $W/\sqrt{Hz}$ at $\lambda = 0.4$ μm have been obtained on these devices. Overall, these detectors have clearly demonstrated the capability of GaP photodiodes for high sensitivity for future use in a star sensor.

FOREWORD

This is the Final Technical Report of the Gallium Phosphide Star Position Sensor Program. This program was sponsored by the Air Force Systems Command, Air Force Avionics Laboratory, Wright-Patterson Air Force Base, Ohio, under Contract No. F33615-75-C-1041. This work was performed from July 1, 1975 through April 30, 1976. The Project Engineer was Dr. R. A. Rotolante and Principal Investigator was Dr. A.M. Chiang. The Program Manager was J.R. Farrell. Acknowledgements are due to Mr. J. Gelpey who helped supervise the fabrication and testing of the GaP photodiodes. Thanks are also due to Mr. B. Denley who fabricated most of the detectors and Mr. R. Healey who obtained most of the test data. The Program Contract Monitor, Mr. Charles Ennis, provided considerable technical direction during the course of the program.

SUMMARY

Mg^+ ion implanted GaP p^+ on n-junction photodiode detectors have been developed for star sensor applications. The sensitivity (NEPs) of these detectors in the wavelength region between 0.34 to 0.48 μm are better than UV enhanced Si photodiodes. For example, an NEP as low as 1.6 x 10^{-14} W/$\sqrt{Hz}$ and a quantum efficiency of 40% has been obtained on these detectors at 0.44 μm. No 1/f noise has been observed on these diodes.

TABLE OF CONTENTS

LIST OF ILLUSTRATIONS

LIST OF TABLES

vi

SECTION I

INTRODUCTION

This is the final technical report under AFAL Contract No.
F33615-75-C-1041. The specific objectives of this program were to fabricate,
test and deliver five single-element (detector size 0.01 x 0.01 inch^2) gallium
phosphide photovoltaic detectors with performance design goals (for each element)
of $\eta > 30\%$ and NEP $\leq 2.5 \times 10^{-14}$ W/$\sqrt{Hz}$ at $\lambda = 0.4$ µm. These detectors are
intended as a feasibility sample for eventual development of arrays and,
finally, reach-through avalanche photodiodes for use in a synchronous orbit,
strapdown star sensor. Additionally, photoconductive test samples were
fabricated in order to evaluate the characteristic of copper-doped GaP
crystals prepared by the Corporate Research Center under AFML funding.

The work effort under this contract resulted in the production,
test and delivery of five high performance Mg$^+$ ion implanted GaP photovoltaic
detectors. Four of the five detectors shipped have a NEP less than
1.6×10^{-14} W/$\sqrt{Hz}$, which well exceeds the specification. The fifth device
has a NEP of 3.6×10^{-14} W/$\sqrt{Hz}$.

Use of ion implantation to incorporate dopants into semiconductors
has proven to be extremely useful for many applications[1,2]. Principally,
implantation allows accurate control of both the doping concentrations and
profiles. It also yields a high purity doping source because the implanted
specie is selected with a mass analyzer. This is in direct contrast to a
diffusion process in which all the impurities present in the furnace, or
contaminants on the semiconductor surface, will diffuse into the crystal
along with the desired dopant.

Recently, there have been a number of studies of ion implantation
in GaP.[3-12] Most previous workers were interested in incorporating optically
active impurities into GaP by ion implantation as a possible fabrication
technology for light emitting diodes. Cathode luminescence from Zn-0 pairs
generated by oxygen implanted into Zn-doped Gap has been observed by Lacey,
et. al.[3] An investigation of nitrogen implantation in GaP[4] showed that
a large substitutional concentration of nitrogen could be achieved, but the
luminescence intensity was $\leq$ 1% of that obtained using conventional doped
crystals having comparable nitrogen concentration. Merz et. al.[5,6]
investigated photoluminescence from the Bi isoelectron trap implanted into
GaP for various ion doses and anneal conditions. For the optimum dose and
anneal, one observed only $\sim$ 10% of the light intensity expected from
the estimated number of substitutional ions. The above results indicated
that the performacne of light emitting diodes made from the ion implantation
can be seriously affected by the lattice damage introduced during the implant
process. Therefore, a rather extensive study of the nature of the implant-
induced damage and the recovery of the damaged crystal as a result of annealing
during and after implantation in GaP has been carried out by many workers.[7-11]

1

In spite of these rather extensive investigations of ion implantation in GaP, until recently, little or no work has been devoted to the use of ion implantation in GaP as a possible fabrication technique for photosensitive devices, such as UV to visible photovoltaic detectors. T. Inada et. al.[12] observed the photovoltaic effect of Mg and Zn implanted into sulfur doped GaP junctions. The purpose of their photovoltage measurement was to determine the junction depth, i.e., the open circuit voltage of the p-n junction was measured by illuminating the implanted surface and followed by a layer removal process. The depth of the junction was determined as the depth where the photovoltage disappeared. No quantitative photoresponse measurement of the ion implanted junction was reported.

In GaP, the value of absorption coefficient, α, rises rapidly for photons with energy above the direct bandgap, $E_g = 2.8$ eV. For example, $\alpha = 7 \times 10^4$ cm^{-1} at 3.1 eV and a shallow junction is required to collect all the photon generated electron-hole pairs. This shallow junction can be achieved by using ion implantation technology.

During the course of this program, the process of Mg^+ ion implant into n-type undoped GaP to form a p-n junction for photon detection was developed and optimized. Combinations of implant ion energies, doses and annealing conditions were investigated. The optimum process, defined here as that which provides low leakage current and high collective quantum efficiency at 0.4 μm, was established. During this program, we observed that the successful application of ion implantation to GaP depends critically on an ability to control the surface composition during the post-heat treatment which is needed to anneal out the radiation damage and to activate the implanted ions.

We have observed that the implantation induced lattice damage in GaP leads to the creation of an amorphous layer on the substrate material. However, post-anneal at $\geq 850^o$C is sufficient to allow the amorphous layer to regrow epitaxially onto the substrate and to restore the lattice structure of GaP to monocrystalline form. After implantation, the implanted impurities are probably at the interstitial lattice sites and, therefore, not capable of contributing to the electrical activities in the normal manner. Post-heat treatment is required to move the ions to substitutional sites and to be electrically active. At an anneal temperature of 850^oC, enough implanted Mg^+ ions are activated to form a p-n junction structure and detectors with NEP as low as 1.6×10^{-14} W/$\sqrt{Hz}$ at 0.4 μm have been observed. However, the electrical properties of the implanted layer, such as mobility and carrier concentration as a function of heat treatment during and after implantation requires further investigation.

Section 2 describes the device design and fabrication process developed during this program. The electrical and optical properties of the implanted junction are discussed in Section 3. Finally, the test report of the five delivered junction diodes is included as Appendix A.

2

SECTION II

DESIGN AND FABRICATION

1.   Device design. The design goal of this program is a GaP pn junction detector with quantum efficiency of 30% at $\lambda = 0.4$ μm. The absorption coefficient, α, of GaP at that photon energy is about $7 \times 10^4 \text{cm}^{-1}$, see Figure 1, which corresponds to an absorption length of 0.14 μm. Therefore, a rather shallow junction is required to collect the photon generated electron-hole pins.

Under steady-state conditions, the total short-circuit current density of a p on n junction is given by:

$$J_{tot} = J_{diff,n} + J_{dr} + J_{diff,p} \tag{1}$$

where $J_{diff,n}$ is the electron diffusion current density due to carriers generated in the p^+ region. J_{dr} is the drift current due to carriers generated in the depletion region, and $J_{diff,p}$ is the hole diffusion current density due to carriers generated in the bulk of the semiconductor (See Figure 2).

Let us now derive the diffusion current from the surface region (p^+). The motion of the photogenerated minority carriers (electrons) in the layer is governed by:

$$\frac{J_{diff,n}}{q} = D_e \frac{d}{dx} n \tag{2}$$

$$-\frac{d}{dx} \left(\frac{J_{diff,n}}{q} \right) = \alpha_\lambda \Phi_o (1-R) e^{-\alpha_\lambda x} - \frac{n-n_o}{\tau_e} \tag{3}$$

where μ_e, τ_e, D_e are electron mobility, lifetime and diffusivity, respectively, Φ_o is the monochromatic incident flux (photons/cm^2-s), α_λ,R are the absorption coefficient and reflectance at the incident wavelength λ, respectively, and n_o is the carrier density at thermal equilibrium. The above minority diffusion equation can be solved analytically with the assumption that D_e, μ_e, τ_e, are constant throughout the surface layer and the boundary conditions:

1) at the surface, $x = 0$

$$\frac{J_{diff,n}}{q} = sn \tag{4}$$
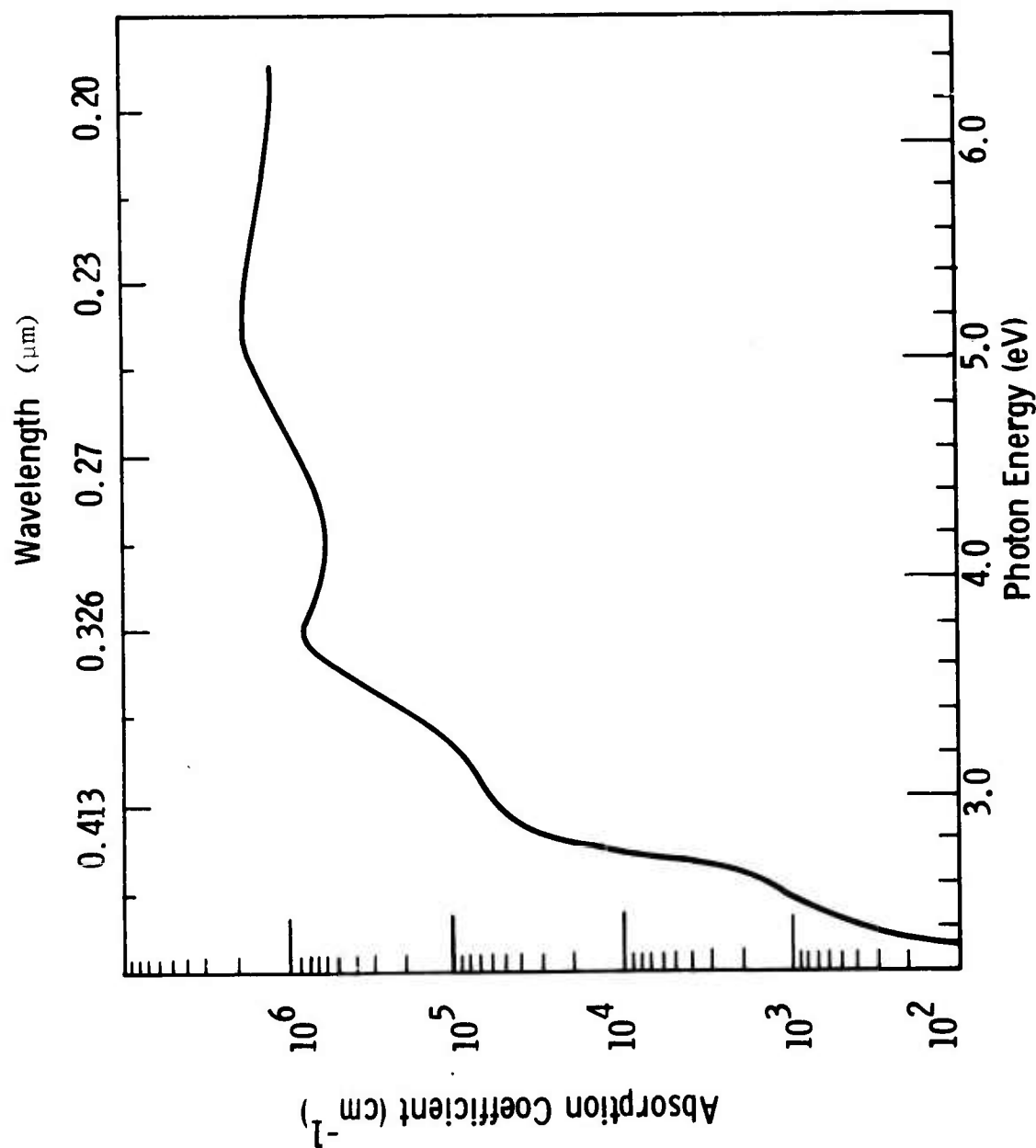
From 2.2 eV to 4.2 eV
based on data by
S. Wemple, et al

From 4.2 eV to 6.4 eV
based on data by
H. Philipp & H. Ehrenreich

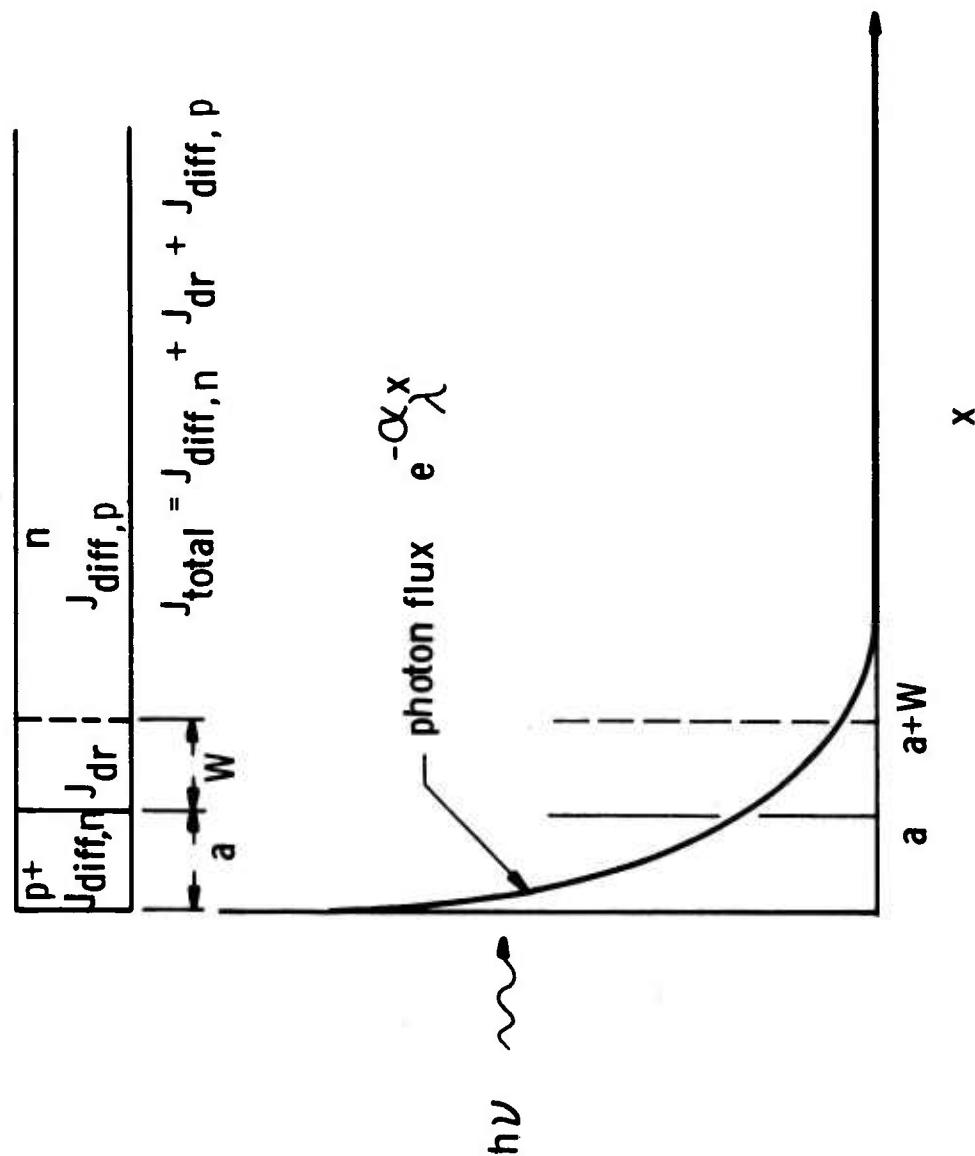Figure 1   ABSORPTION COEFFICIENT DATA IN GaP

4

$$J_{total} = J_{diff,n} + J_{dr} + J_{diff,p}$$

p+ | n

$J_{diff,n}$ J_{dr} $J_{diff,p}$

a W

photon flux $e^{-\alpha_\lambda x}$

hν

a   a+W

x

Figure 2   LIGHT INTENSITY VERSUS DISTANCE IN A p-n JUNCTION PHOTODIODE WHERE W IS THE DEPLETION WIDTH AND a IS THE JUNCTION DEPTH

5

where s is the surface recombination velocity:

2) at the junction interface, $x = a$,

$$n = 0 \tag{5}$$

The diffusion current density from the p region into the depletion region can be expressed as

$$J_{diff,n} = Q\alpha_\lambda \, e^{-\alpha_\lambda a} + \frac{Q}{L_e} \, e^{-\alpha_\lambda a} \; \frac{\dfrac{S}{D_e} \, \cosh \dfrac{a}{L_e} + \dfrac{1}{L_e} \, \sinh \dfrac{a}{L_e}}{\dfrac{S}{D_e} \, \sinh \dfrac{a}{L_e} + \dfrac{1}{L_e} \, \cosh \dfrac{a}{L_e}}$$

$$- \frac{\dfrac{Q}{L_e} \left(\dfrac{S}{D_e} + \alpha_\lambda \right)}{\dfrac{S}{D_e} \, \sinh \dfrac{a}{L_e} + \dfrac{1}{L_e} \, \cosh \dfrac{a}{L_e}} \tag{6}$$

where:

$$Q = \frac{-q\alpha_\lambda \, \phi_0 \, (1-R)}{\alpha_\lambda^2 - L_e^{-2}} \quad ; \qquad L_e = \sqrt{\tau_e D_e} \quad \text{is the electron diffusion length} \tag{7}$$

The drift current in the depletion region is given by:

$$J_{dr} = \int_a^{a+W} \alpha_\lambda \Phi_o (1-R) e^{-d_\lambda x} \, dx, \text{ where W is the depletion width.}$$

It is straightforward to derive:

$$J_{dr} = q\phi_0 \left[e^{-\alpha_\lambda a} - e^{-\alpha_\lambda (a + W)} \right] (1-R) \; . \tag{8}$$

Similarly, one can derive the diffusion current from the n region into the depletion region, that

$$J_{diff,p} = Q' e^{-\alpha_\lambda (a + W)} \left[\frac{1}{L_p} \coth \left(\frac{d-a-W}{L_p} \right) - \alpha_\lambda \right] - Q' \frac{e^{-\alpha_\lambda d}}{L_p \, \sinh \left(\dfrac{d-a-W}{L_p} \right)} \tag{9}$$

6

where:

$$Q' = \frac{-q\alpha_\lambda \phi_0 (1-R)}{\alpha_\lambda^2 - L_p^{-2}} \qquad \text{where d is the device thickness} \qquad (10)$$

where d is the device thickness and L_p is the hole diffusion length.

The quantum efficiency of a photodiode is defined as:

$$\eta = \frac{J_{tot}}{q\phi_0} = \frac{J_{diff,n} + J_{dr} + J_{diff,p}}{q \ \phi_0} \qquad (11)$$

Using the material parameters listed in Table 1, quantum efficiency at 0.4 μm of an ion implanted GaP photodiode has been calculated:

$$\eta \simeq (0.5 + 0.26 + 0.02)(0.62) = 0.47 \qquad (12)$$

One can see that, with a shallow junction, over 40%, quantum efficiency at 0.4 μm of a GaP photodiode can be achieved.

Table 1

GaP MATERIAL PARAMETERS USED IN CALCULATION OF EQUATION (12)

$L_e = 0.5$ μm	$L_h = 0.5$ μm
$D_e = 2.58$ cm^2/s	$D_h = 1.4$ cm^2/s
$S = 1 \times 10^5$ cm/s	$\alpha_{0.4\ \mu m} = 7 \times 10^4$ cm^{-1}
$a = 0.15$ μm	$W = 0.2$ μm
$N_d = 5 \times 10^{16}$ cm^{-3}	$R = 0.38$
$d = 300$ μm	

2.   Process consideration. The major process considerations in constructing an ion implanted GaP photodiode are: (1) the range-energy relation of the implant ions for achieving the desired junction depth, impurity concentrations and profile; (2) the proper heat treatment during and after implant to anneal the implant induced crystal damage and to activate the implant impurity.

7

Junction depth can be predicted with relative accuracy from range energy calculation using a computer program developed by Johnson and Gibbons,[14] which is based on the LSS theory.[15] The projected range, R_p, and the range struggling, ΔR_p, of Mg^+ in GaP are plotted in Figure 3, as a function of implant energy. According to LSS theory, the implanted ions in the substrate follows a Gaussian distribution i.e., the concentration $N(x)$ of implanted ions at depth x from the surface is given by:

$$N(x) = N_{max} \, e^{-1/2 \left(\dfrac{x - R_p}{\Delta R_p} \right)^2} \tag{13}$$

In equation (13), N_{max} is the peak concentration of the profile corresponding to $x = R_p$, i.e.:

$$N_{max} = \frac{Q_s}{\sqrt{2\pi} \, \Delta R_p} \tag{14}$$

where Q_s is the implant dose. Figure 4 shows the predicted Mg^+ distribution in GaP for two implant energies. Note, these computed values are based on the assumption that the implant ions are 100% substitutional in the lattice site and electrically activated. The implant dose and implant energy used in the figure represent the approximate region of interest in this program to produce a shallow, abrupt p^+ on n junction.
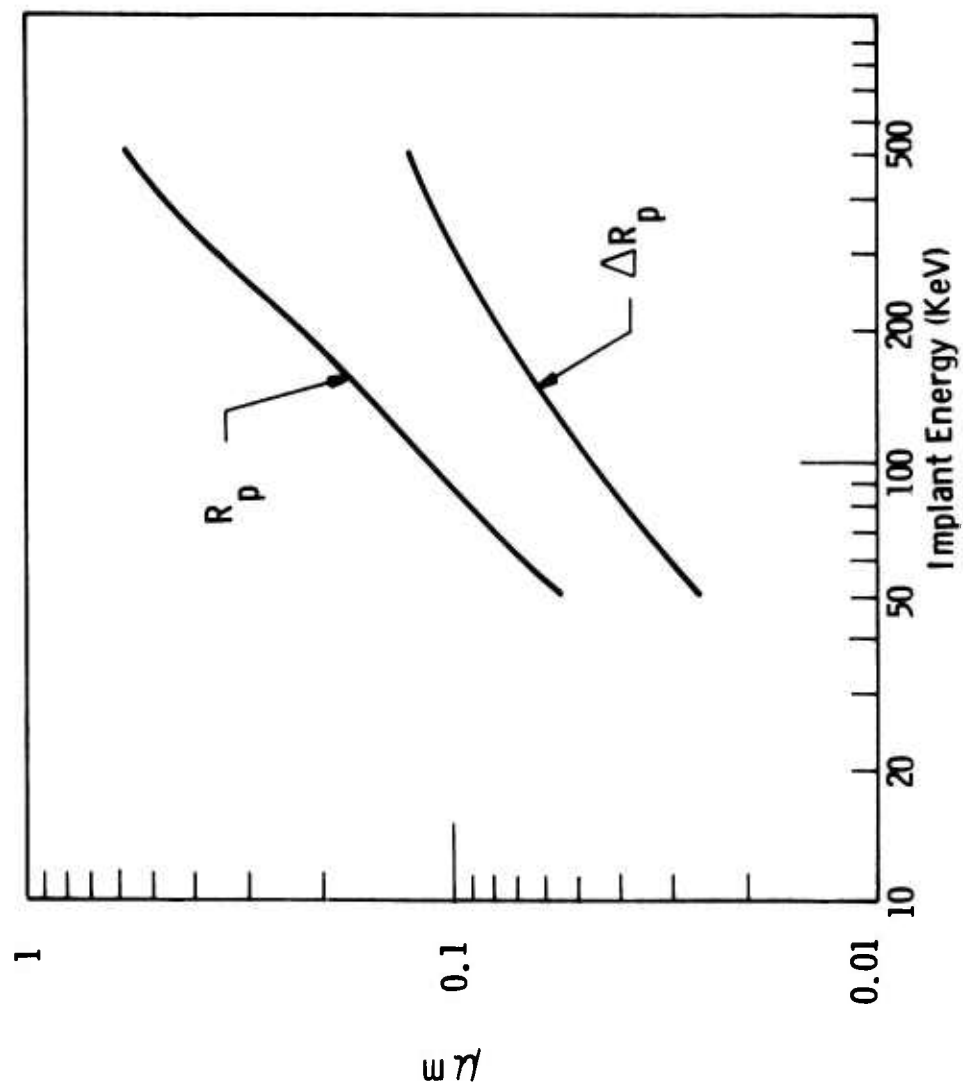
Figure 3   THE PROJECTED RANGE R_p, AND THE STANDARD DEVIATION ΔR_p of Mg IONS IN GaP
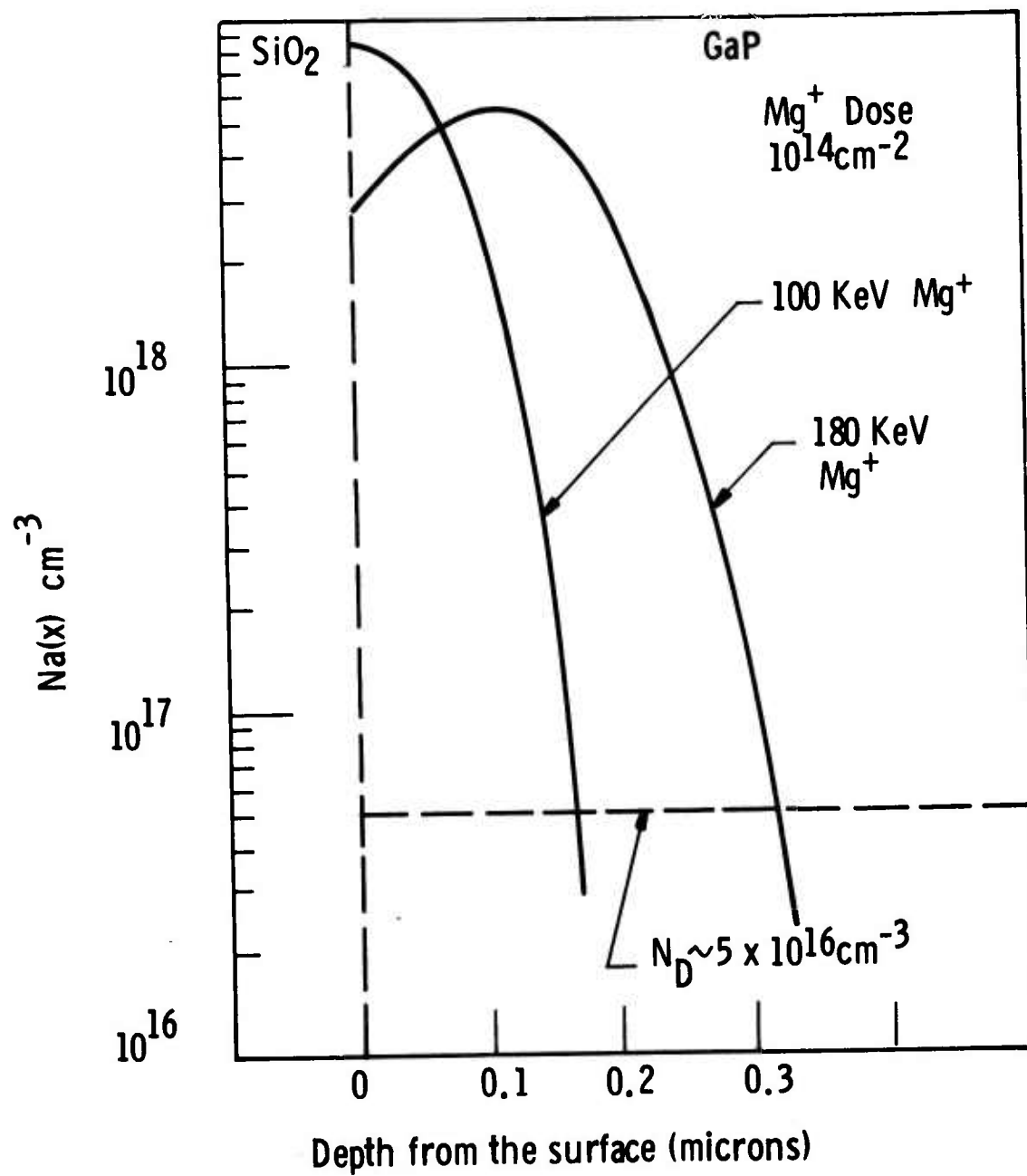
9

Figure 4   ION IMPLANTED DISTRIBUTION PROFILE FOR Mg$^+$ IN GaP

SECTION III

ELECTRICAL AND OPTICAL PROPERTIES

1.   Detector testing and selection procedure.   In this program, we
followed the testing and selection schedule shown in Figure 5.   After ion
implementation and post annealing at $\geq$ 850°C, wafers were inspected under
a 100X microscope.   Only those wafers with a relatively smooth and pit-free
surface were processed further.   Badly decomposed wafers due to poor oxide
coating were rejected at this point.

After a p-n junction diode was completely fabricated, a probe
station was used to measure the current-voltage characteristics and short
circuit photocurrent of the diode through a Tektronix Curve Tracker Model
576.   Based on these initial measurements, those diodes exhibiting reasonably
good characteristics were mounted on dual-in-line packages and subjected
to further testing of detector properties, including spot scan of the detector
sensitive area, spectral response, noise, I-V and NEP.   Finally, the five
best detectors were selected and delivered to AFAL.

2.   p-n junction detector performance

a.   Spot scan of detector sensitive area.   The detector area and
uniformity were determined by raster scanning the detector with a sharply
focused Tungsten source (spot size 0.001 inch).   A typical detector pattern
is shown in Figure 6.   One can see that the detector response across the
sensitive area is very uniform.   The dip in the off-center area corresponds
to the front contact pad and one mil gold wire.   The implant mask was a 13
mil diameter circular pattern.   From the spot scan results, one can see
that no side diffusion of the implanted ions were observed after annealing
at 850°C or higher temperature.

b.   Spectral response.   The spectral response of ion implanted GaP
p-n junction photodiodes was measured by using a Tungsten source and a Jarrel
Ash 0.25 meter monochrometer.   An EG&G calibrated Si detector (530-2) was
used to calibrate the light source.

Peak response of those diodes is around 0.445 μm as shown in Figures
7, 8, and 9.   At $\lambda = 0.4$ μm, efficiency of 28% has been measured. Cal-
culated quantum efficiencies at 0.4 μm as a function of surface recombination
velocity based on equation 7 and actual fabrication parameters were plotted
in Figure 10, where two different minority (electron) diffusion lengths
were used.   Compared with the measured data, it revealed that the surface
recombination velocity of those ion implanted GaP photodiode is larger than
10^5 cm/s, and the minority carrier diffusion length in the implanted region
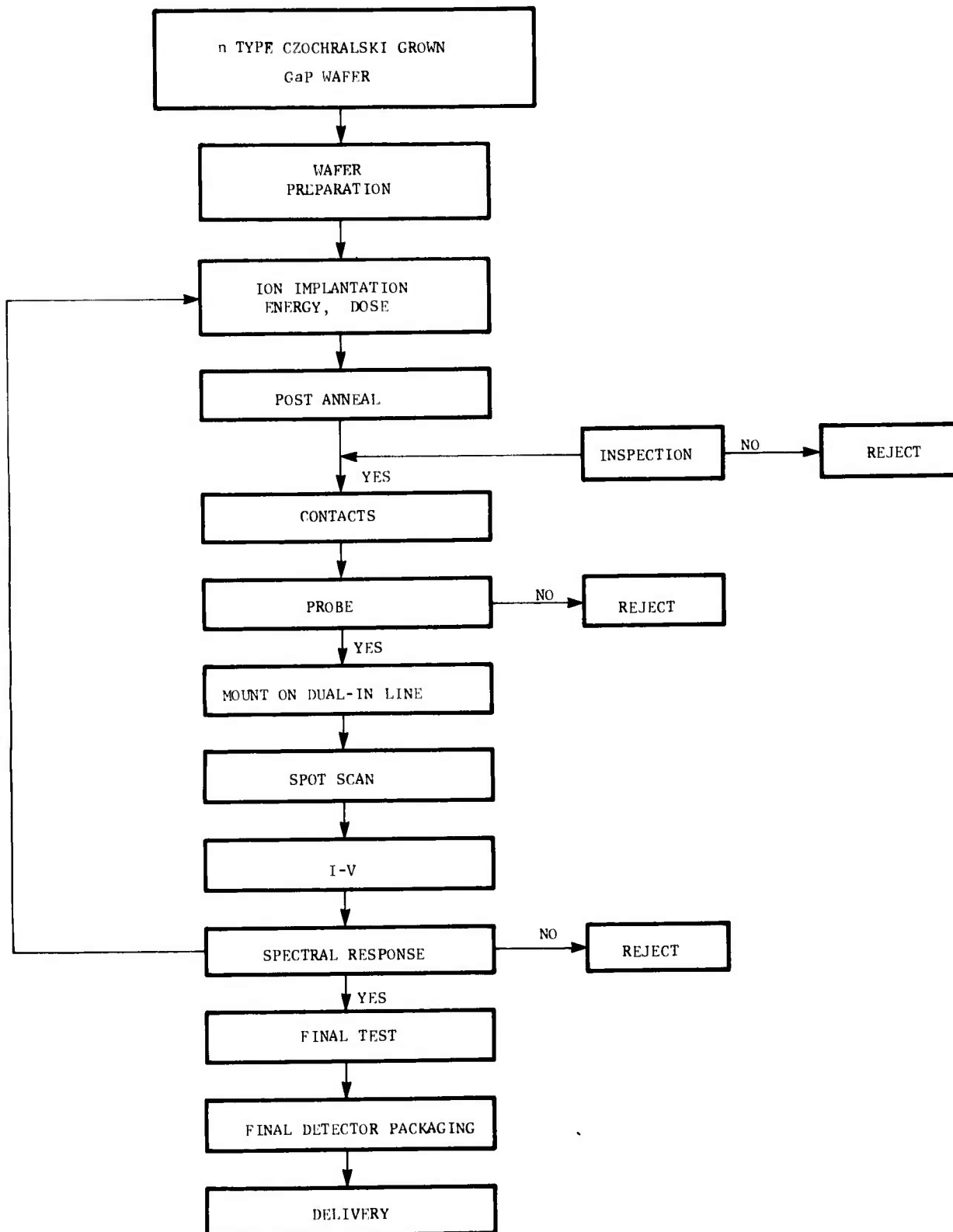is about 0.1 μm.   Assuming an electron mobility of 100 cm^2/V-s, it corresponds

11

Figure 5   TESTING AND DELIVERY OF SCHEDULE FOR GaP ION
IMPLANTED PHOTODIODES

12

Figure 6 SPOT SCAN OF DETECTOR #3
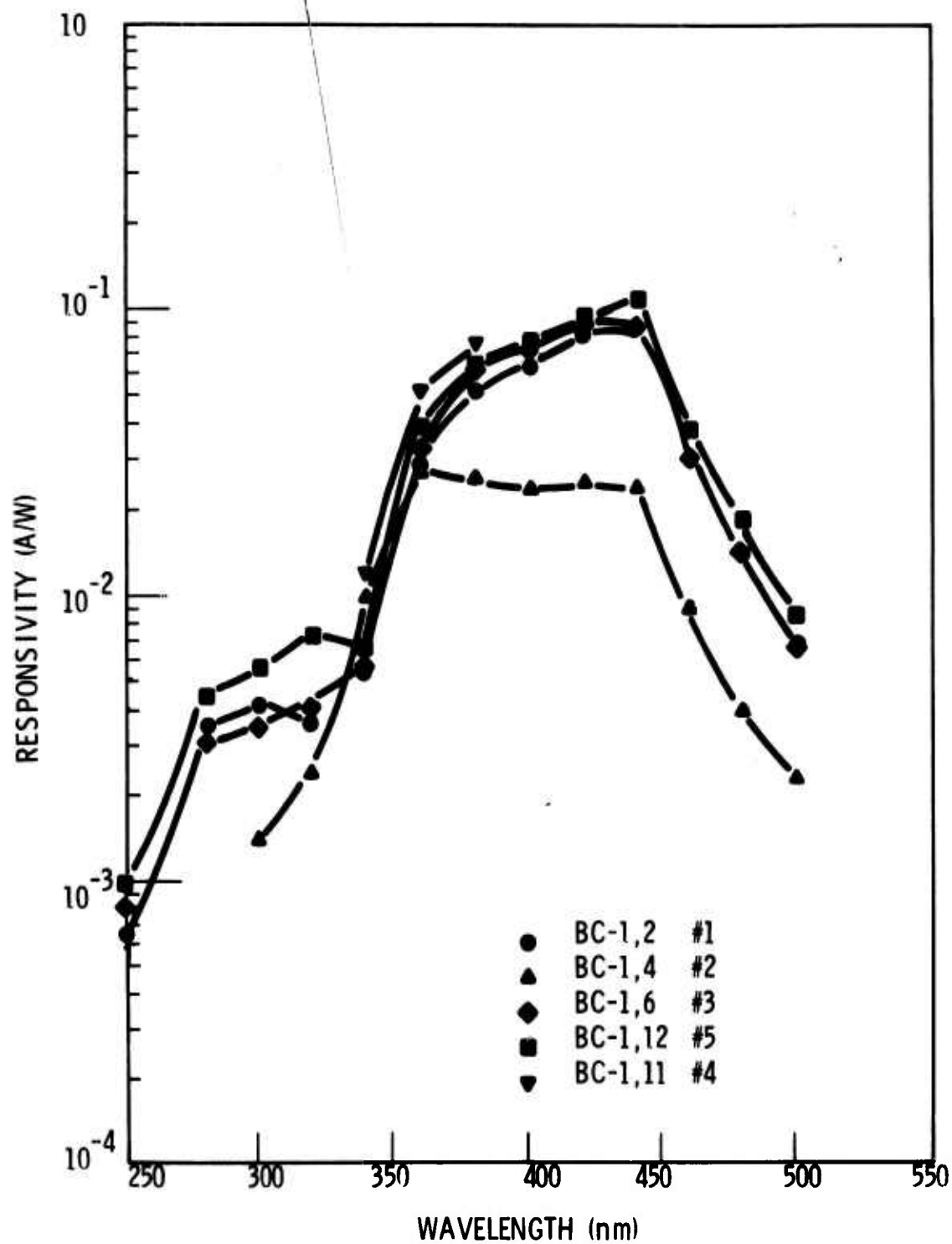
GaP BC-1,6

0.001"

Figure 7   SPECTRAL RESPONSES OF ION IMPLANTED GaP JUNCTION
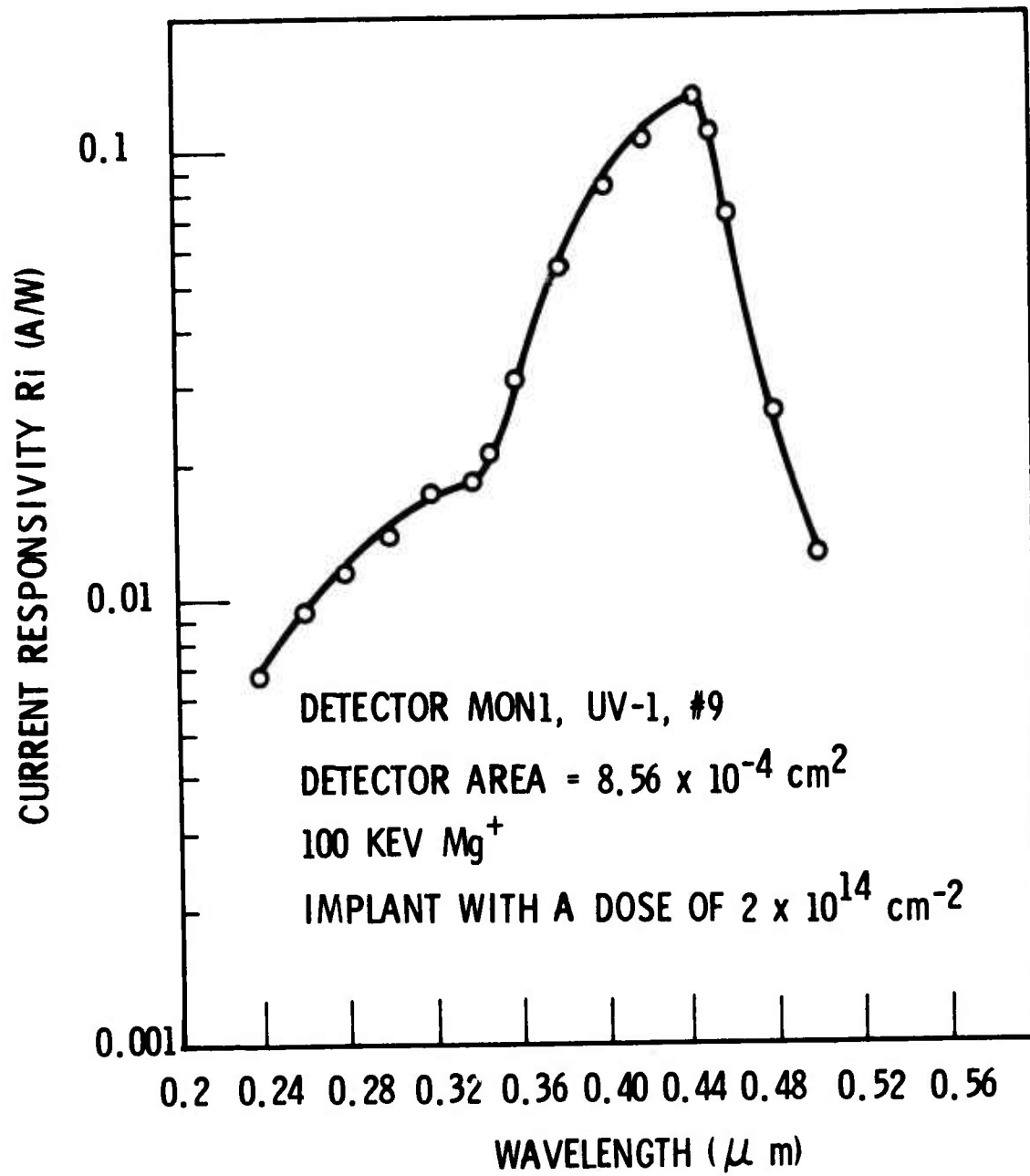DETECTORS

14

Figure 8   SPECTRAL RESPONSE OF ION IMPLANTED GaP JUNCTION
DETECTOR

Figure 9 SPECTRAL RESPONSE OF ION IMPLANTED GaP JUNCTION DETECTOR

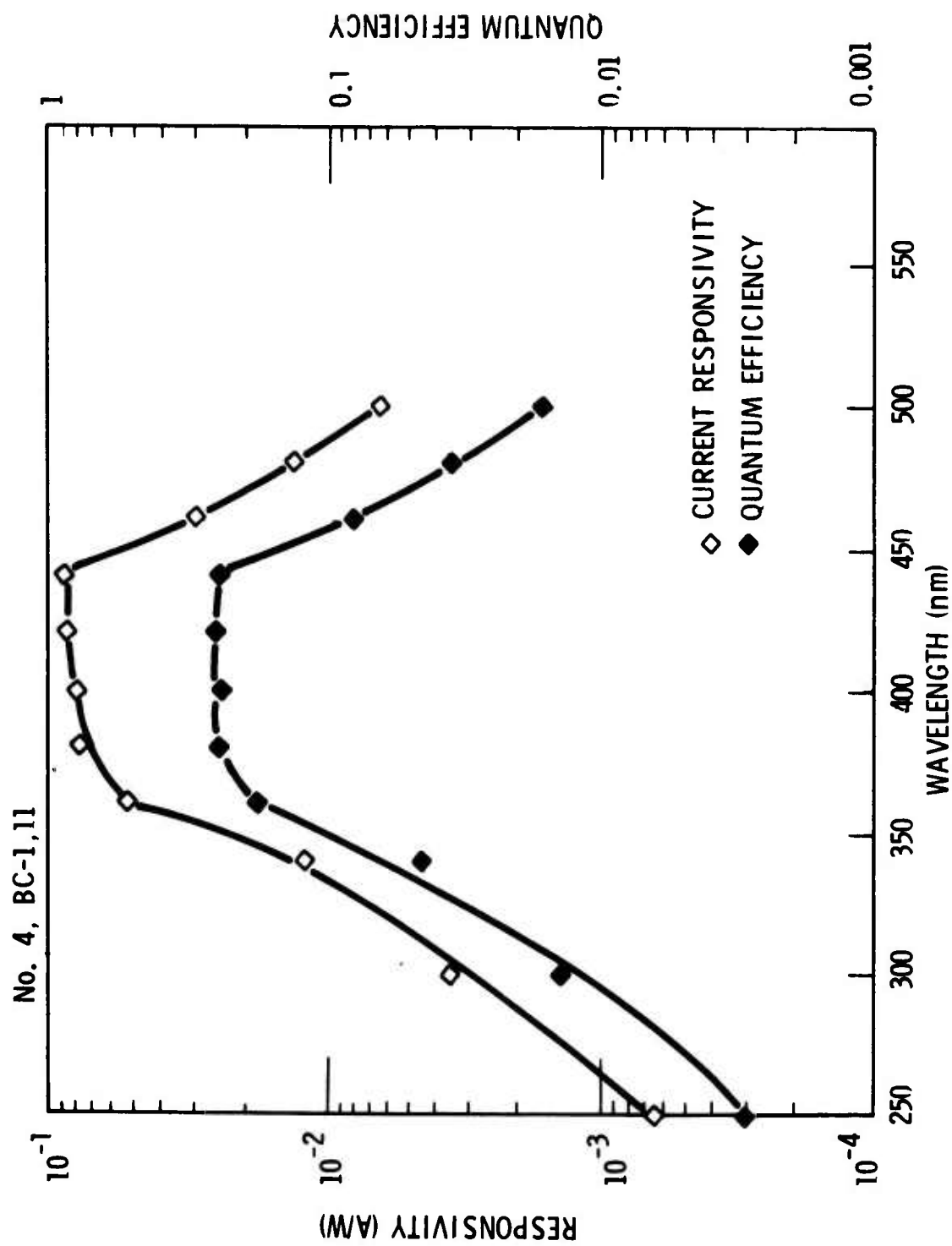16

CALCULATION ASSUMPTION

$\lambda = 0.4 \mu m$ $\alpha_\lambda = 7 \times 10^4 cm^{-1}$

$a = 0.15 \mu m$ $W = 0.2 \mu m$

$D_e = 2.58 \, cm^2/s$ $D_h \approx 1.4 \, cm^2/s$

Calculated η, assume $L_e = 0.5 \, \mu m$

Measurement

Calculated η, assume $L_e = 0.1 \mu m$

Surface Recombination Velocity
(cm/s)

Quantum Efficiency
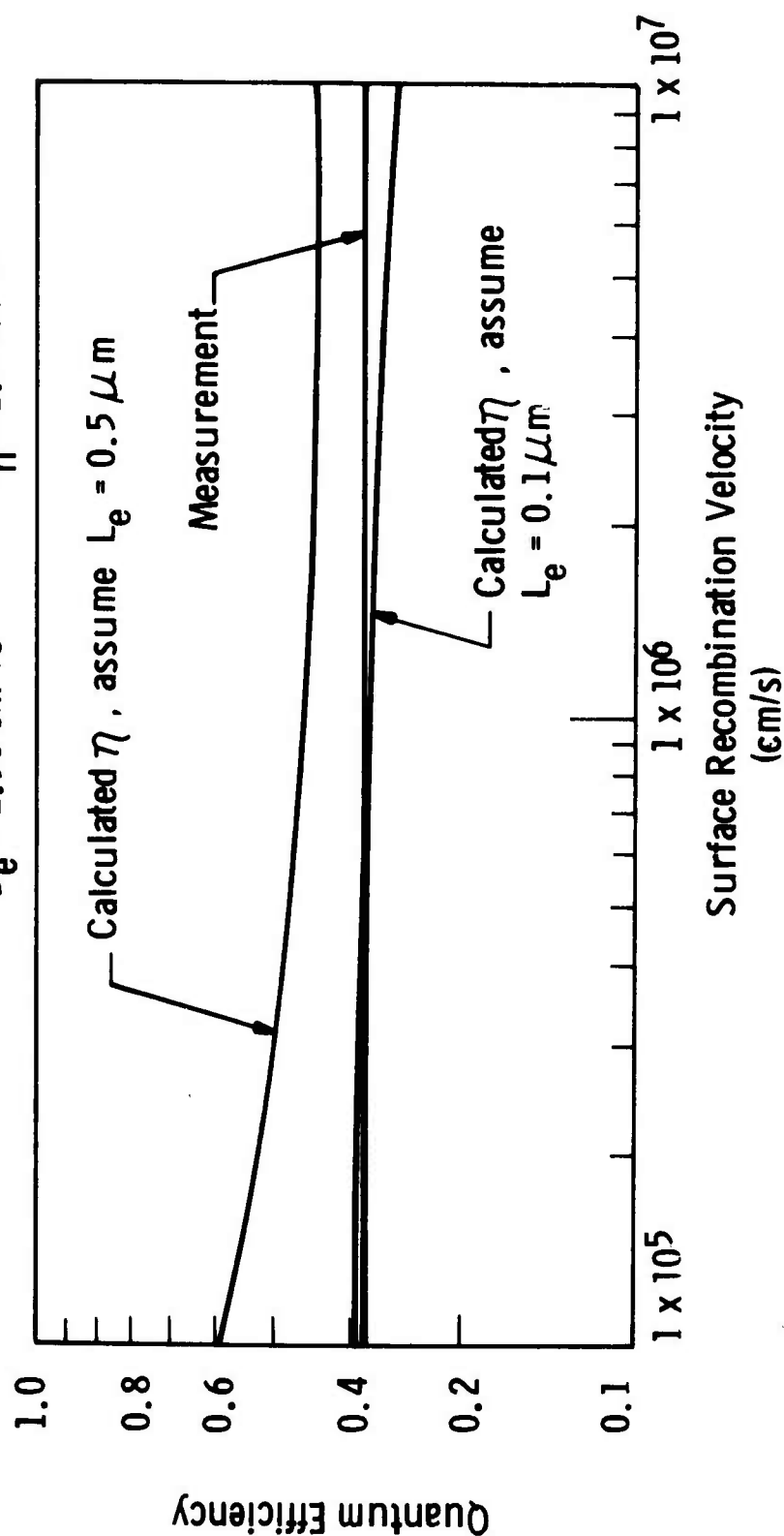
Figure 10   QUANTUM EFFICIENCY VS SURFACE RECOMBINATION VELOCITY

17

to a minority carrier life time of 3×10^{-11} s. From measurement of the minority carrier diffusion length using the technique of Logan and Chynoweth,[17] Epstein and Groves[18] have reported that minority carrier lifetime in epitaxially deposited single crystal gallium phosphide solar cell varies between 10^{-10} and 10^{-12} s.

There are two possible reasons for the relatively fast decrease of the spectral response of those diodes below 0.36 µm. First, high surface recombination velocity, as stated above, would result in a poor device UV response. Secondly, because a Tungsten source was used for the whole range of measurements (0.25 to 0.52 µm), the combined output from the Tungsten light source and stray light background of the monochrometer would yield a false deterioration of the GaP detector performance at wavelengths below 0.36 µm. Improving surface preparation and establishing a built-in electric field in the implanted region by a controlled exponential distributed implanted profile, the high surface recombination problem can be solved. By selecting a source with a limited spectral region (i.e., a deuterium lamp for the UV), the effect of stray light background of the present setup can be eliminated.

c.　　　　Current voltage measurements. The current voltage relation of each detector was measured with a Keithley electrometer. Typical reverse bias I-V characteristics are shown in Figures 11 and 12.

For large reverse bias ($qV_{RB}/kT > 1$), the generation recombination current density in the diode depletion region is:

$$J_{g-r} = \frac{q\,n_i\,W}{2\tau} \tag{15}$$

where W is the depletion width and τ is the effective carrier lifetime. It is straightforward to calculate that for a depletion width of 0.4 µm and effective lifetime of 3×10^{-11} s, the corresponding g-r dark current of diodes fabricated in the present program is about 4×10^{-16} amp.

One can see that, for small area photodiodes, the package leakage current will be a limiting factor in the reversed bias current voltage measurement, as shown in Figure 11.

d.　　　　Noise. Noise spectra of each detector were measured by using a Quantech Model 304. At zero bias, no 1/f noise was observed on these diodes down to 1 Hz (see Figures 13 and 14). At 0.5 volt reverse bias, the observed excess low frequency noise may come from the feedback resistor, since measurement made on similar resistors showed essentially identical excess low frequency noise under bias. At 0.5 V reverse bias, the 1/f noise current knee is about 50 Hz.
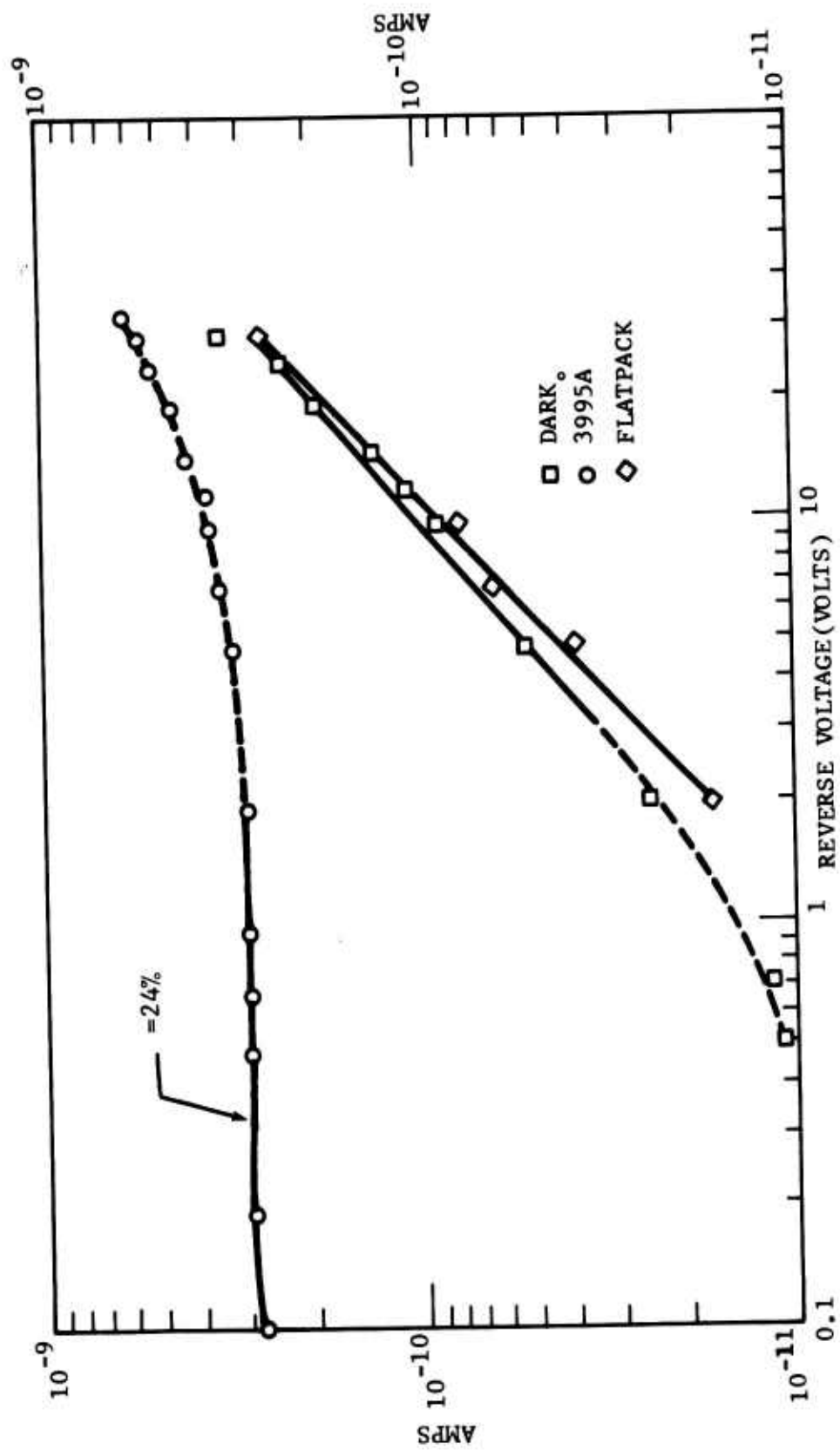
18

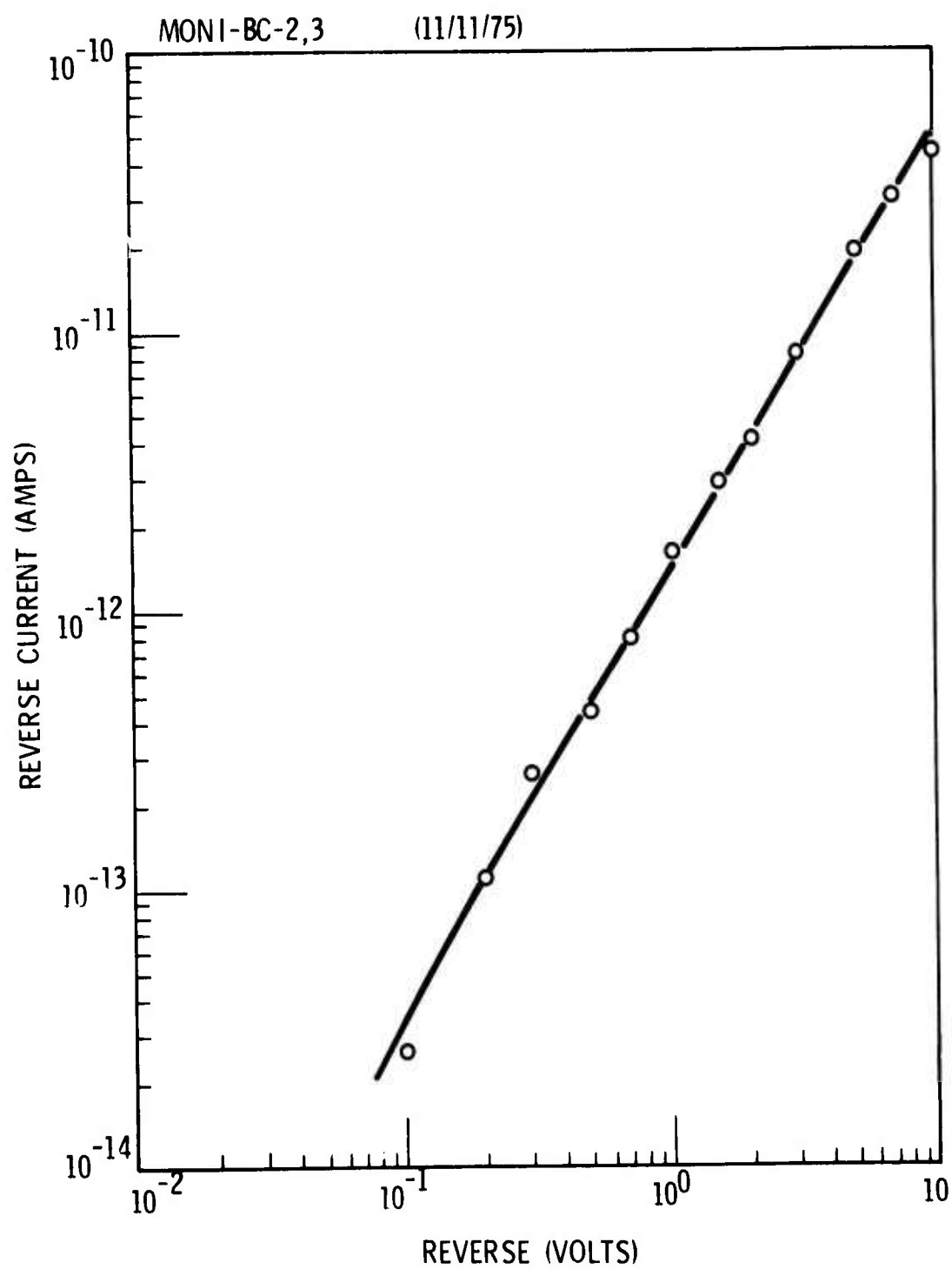Figure 11 REVERSE DARK & LIGHT JUNCTION CURRENT

19

Figure 12   REVERSE DARK JUNCTION CURRENT
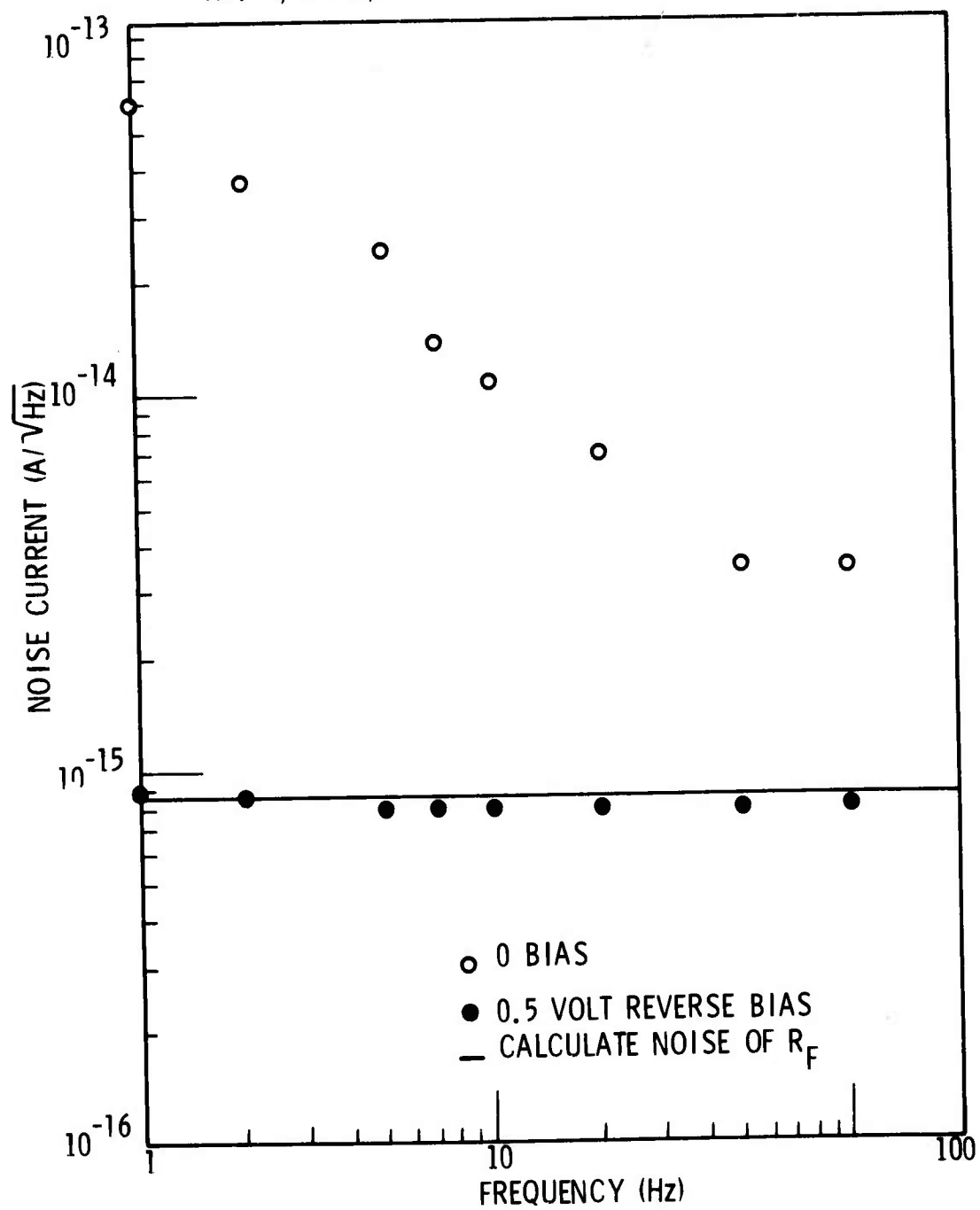
20

No. 2, BC-1,4

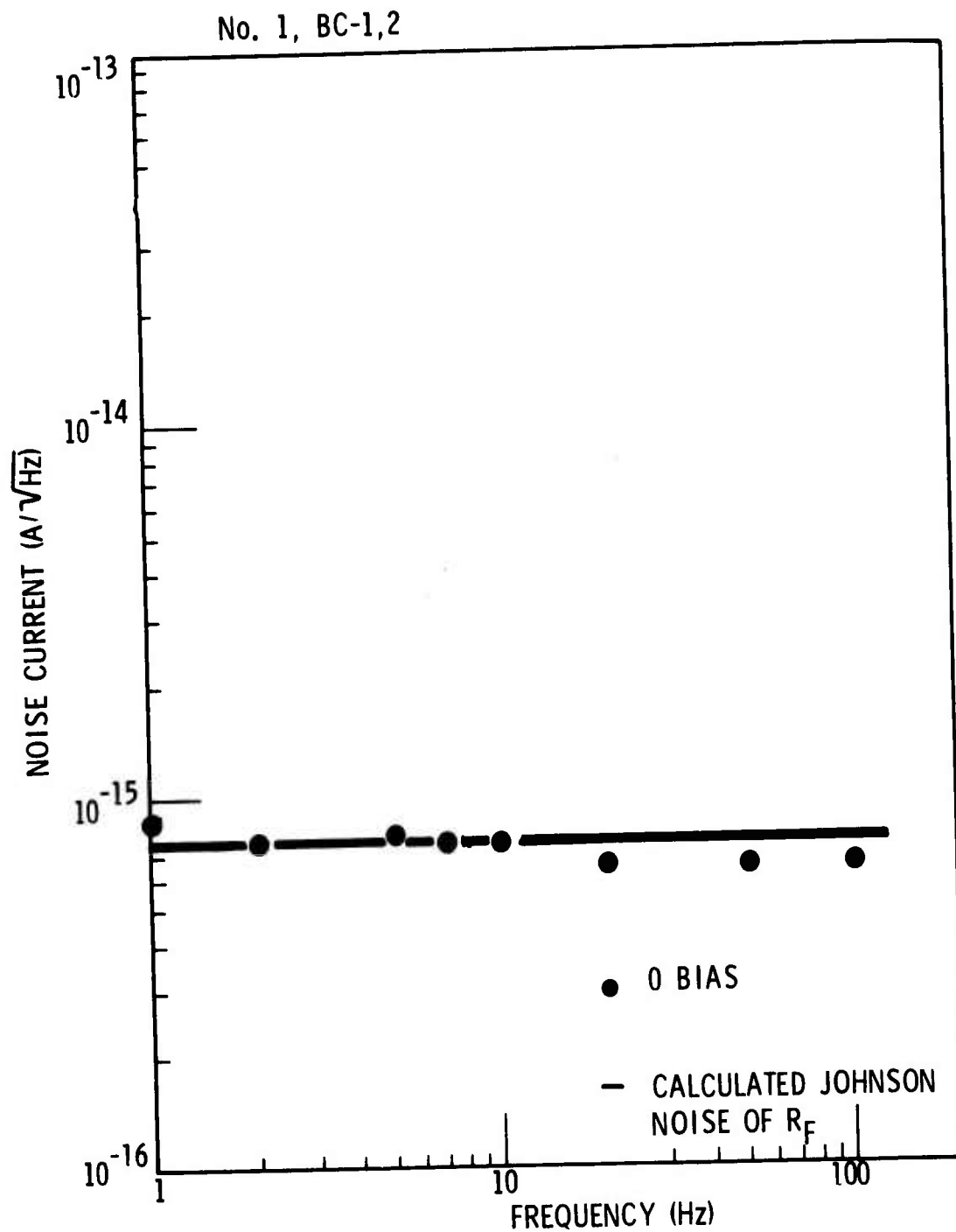Figure 13   DETECTOR NOISE SPECTRUM

21

Figure 14 DETECTOR NOISE SPECTRUM

The equivalent circuit, Figure 15, shows the principal noise source of a photodiode/preamplifier assembly. The total noise of the system can be written as:

$$i_n^2 = i_B^2 + i_{Ro}^2 + i_{sh}^2 + i_{1/f}^2 + i_{na}^2 + i_{R_F}^2 \tag{16}$$

Each of the noise terms is described as follows:

1. Short circuit shot noise from background i_B

$$i_B^2 = 2q \left[2qA \ (Q_S + Q_B) \right]$$

2. Shot noise from the junction dark current i_{Ro}^2

$$i_{Ro}^2 = 2q \ I_o = 2q \left(\frac{q \ n_i \ W \ A}{2\tau} \right)$$

3. Thermal noise of shunt resistance R_{sh}

$$i_{sh}^2 = 4kT/R_{sh}$$

4. 1/f noise

5. Amplifier noise i_{na}^2.

6. Thermal noise from the feedback resistor R_F

$$i_{R_F}^2 = \frac{4kT}{R_F}$$

Since all the noise measurements in this program were carried out in the dark, the background generated noise was eliminated. The temperature dependent noise of a GaP PV/preamplifier system in the dark is plotted in Figure 16. Due to the low intrinsic concentration of GaP, the dark current noise of a GaP device is so low that in practical cases the thermal noise from the 10^{10} ohm feedback resistance is the dominant noise source. One can see that, in Figures 13 and 14, all the measured noise is from the thermal noise of the feedback resistor.
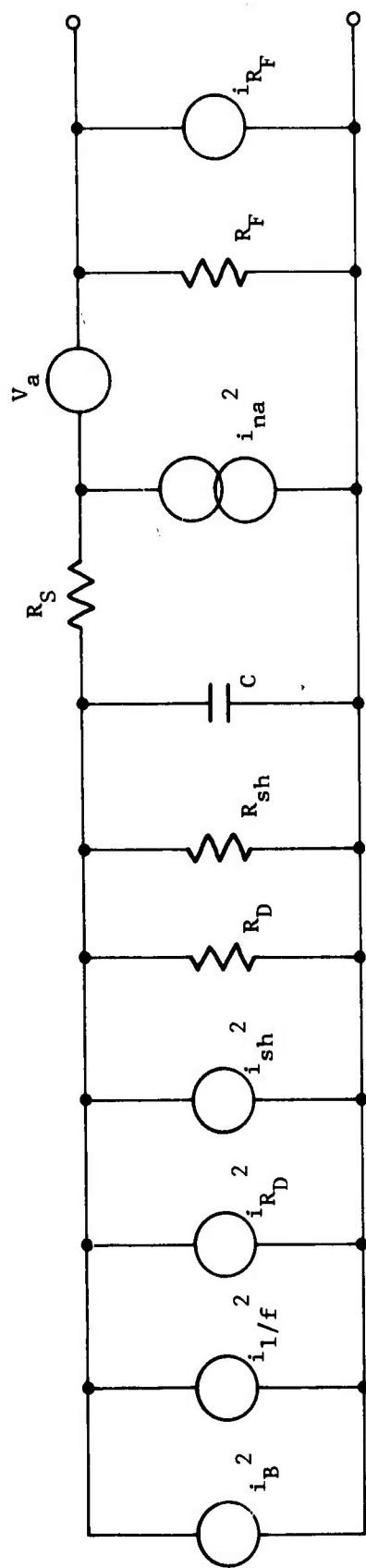
Figure 15 NOISE EQUIVALENT CIRCUIT OF A PHOTOVOLTAIC DETECTOR/PREAMPLIFIER SYSTEM
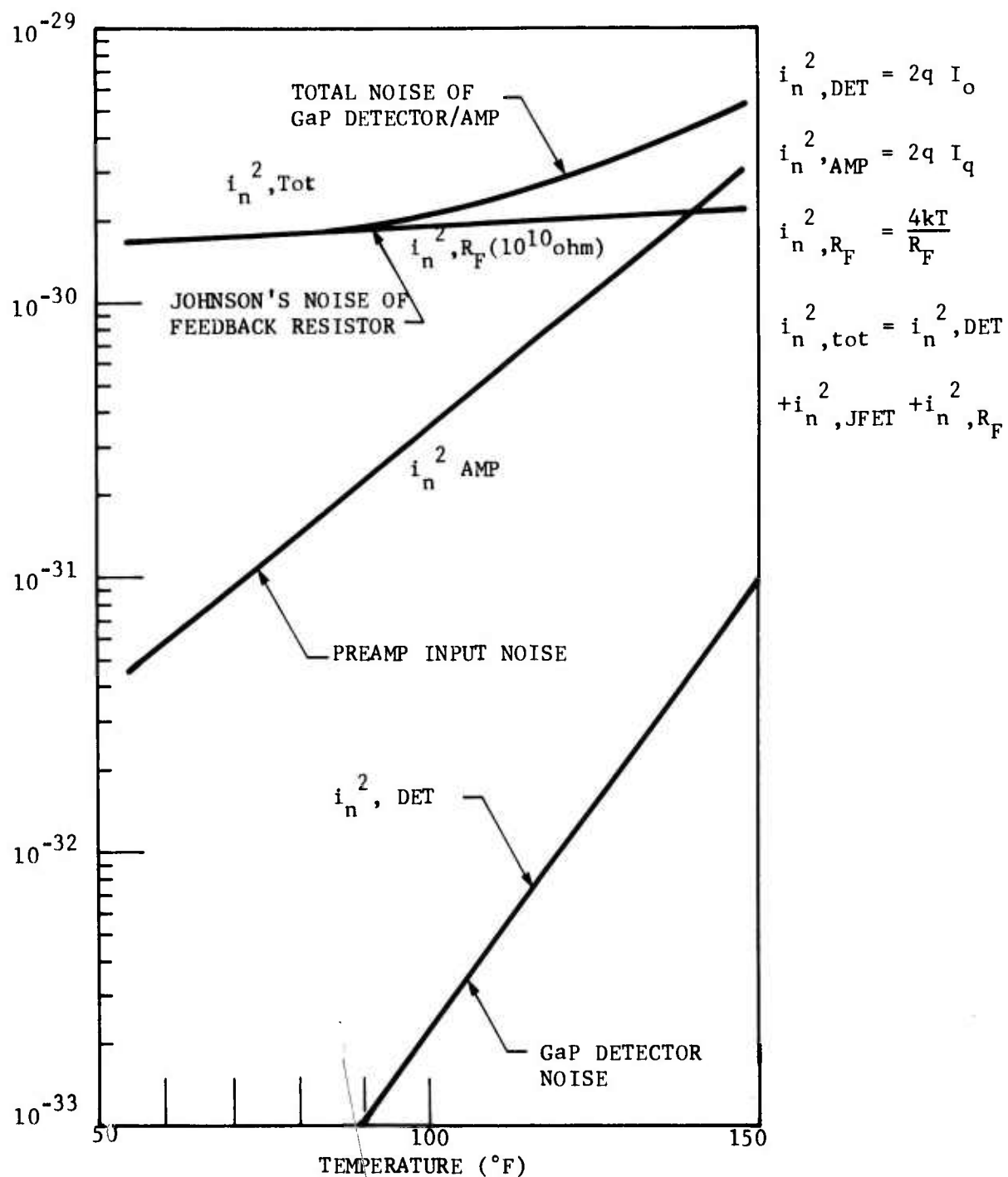
24

Figure 16   NOISE POWER DENSITY VS DETECTOR TEMPERATURE

e.   NEP. The noise equivalent power (NEP), of GaP ion implanted GaP
photodiodes were calculated, based on the equation:

$$NEP = \frac{i_N \, P_{in}}{i_s \sqrt{\Delta f}} \qquad (17)$$

A comparison of Si, GaP and photomultiplier performance data in the 0.2 to
0.6 micrometer region is shown in Figure 17. The high sensitivity of GaP
photodiode detectors in the visible and UV region is clearly demonstrated.
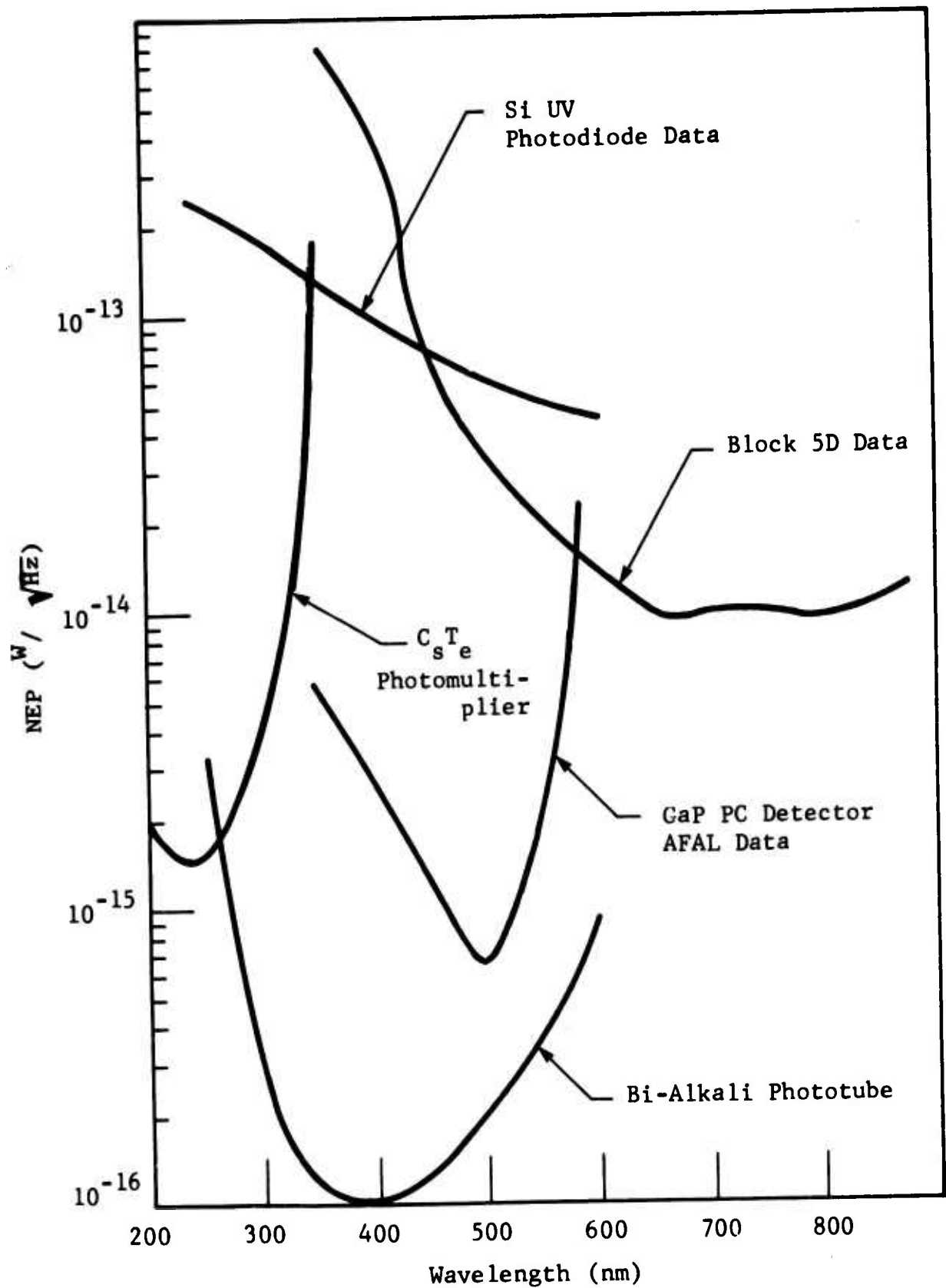
Figure 17   DATA COMPARISON: GaP AND ALTERNATIVE
DETECTORS

27

REFERENCES

1. J.W. Mayer, L. Eriksson and J.A. Davis, Ion Implantation in Semiconductors, (Academic, New York, 1970).

2. G. Dearnaley, J.H. Freeman, R.S. Nelson and J. Stephen, Ion Implantation (North-Holland Publishing Co., Amsterdam, 1974).

3. S.D. Lacey, L.N. Large and D.R. Wright, Elec. Lett, 5, 203 (1970).

4. J.L. Merz, E.A. Sadocoski and J.W. Rodgers, Solid State Commun., 9, 1037 (1971).

5. J.L. Merz, L.C. Feldman and E.A. Sadoioski, Radia, Eff. 6, 285 (1970).

6. L.C. Feldman, W.,. Angustynials and J.M. Merz, Radia. Eff. 6, 293 (1970).

7. J.E. Davey, T. Pankey, P.R. Malmberg and W.H. Lucke, Appl. Phys. Lett., 17, 323 (1970).

8. G. Carter, W.A. Grant, J.D. Haskell and G.A. Stephens, Radia. Damage by Implanted Ions in GaAs and GaP.

9. S.H. Wemple, J.C. North and J.M. Dishman, Journal of Appl. Phys. 45, 1578 (1974).

10. P.M. Hemenger and B.C. Dobbs, Appl. Phys. Lett, 23, 462 (1973).

11. A.B. Campbell, W.A. Grant and G.A. Stephens, Radi, Eff., 17, 19 (1973).

12. T. Inada and T. Ohnuki, Appl. Phys. Lett. 25, 228 (1974).

13. J.F. Gibbons, Proc. of the IEEE, 60, 1062 (1972).

14. W.S. Johnson, J.F. Gibbons, Stanford University Press, Projected Range Statistics in Semiconductors, 1970.

15. J. Lindhand, M. Scharff, H.E. Schmidt, Mat.Fys. Medd. Dan. Vid. Selsk, 33, No. 14 (1963).

16. Technical Report AFAL-TR-75-231.

17. R.A. Logan and A.G. Chynoweth, J. Appl. Phys. 33, 1649 (1962).

18. A.S. Epstein and W.O. Groves, Adv. Energy Conversion, Vol. 5, 161 (1964).

APPENDIX A

TEST REPORT

TABLE OF CONTENTS

SECTION I

TABLE I

DETECTOR DESCRIPTION AND TEST CONDITIONS

Type of Detector	Gallium Phosphide Photodiodes
Detector Size	0.013" diameter
Detector Identification	#1: MON1-BC-1,2
	#2: MON1-BC-1,4
	#3: MON1-BC-1,6
	#4: MON1-BC-1,11
	#5: MON1-BC-1,12
Detector Layout	(see diagram)
Detector Configuration	p^+ on n

Test Conditions

Transimpedance used for tests	2.3×10^{10} Ω
Spectral Radiometer	Calibrated power in 0.012" spot
Spot scan	0.015" spot

Diagram of Pin Connection
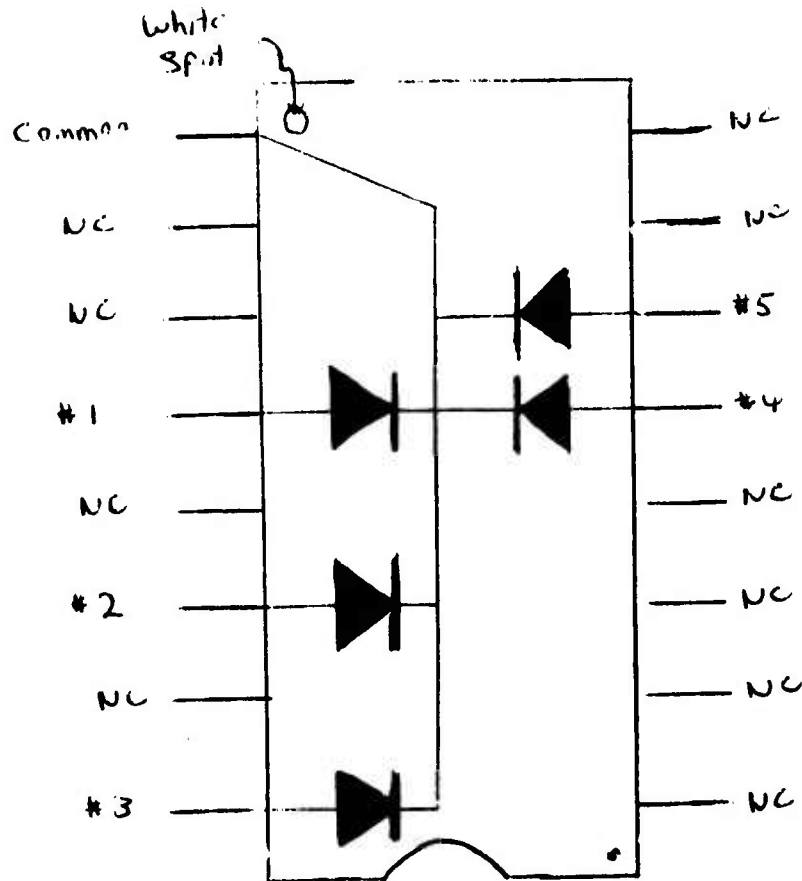
SECTION II

SPECTRAL DATA

FIGURE

Figure 1 COMBINED SPECTRAL DATA OF THE FIVE DETECTORS
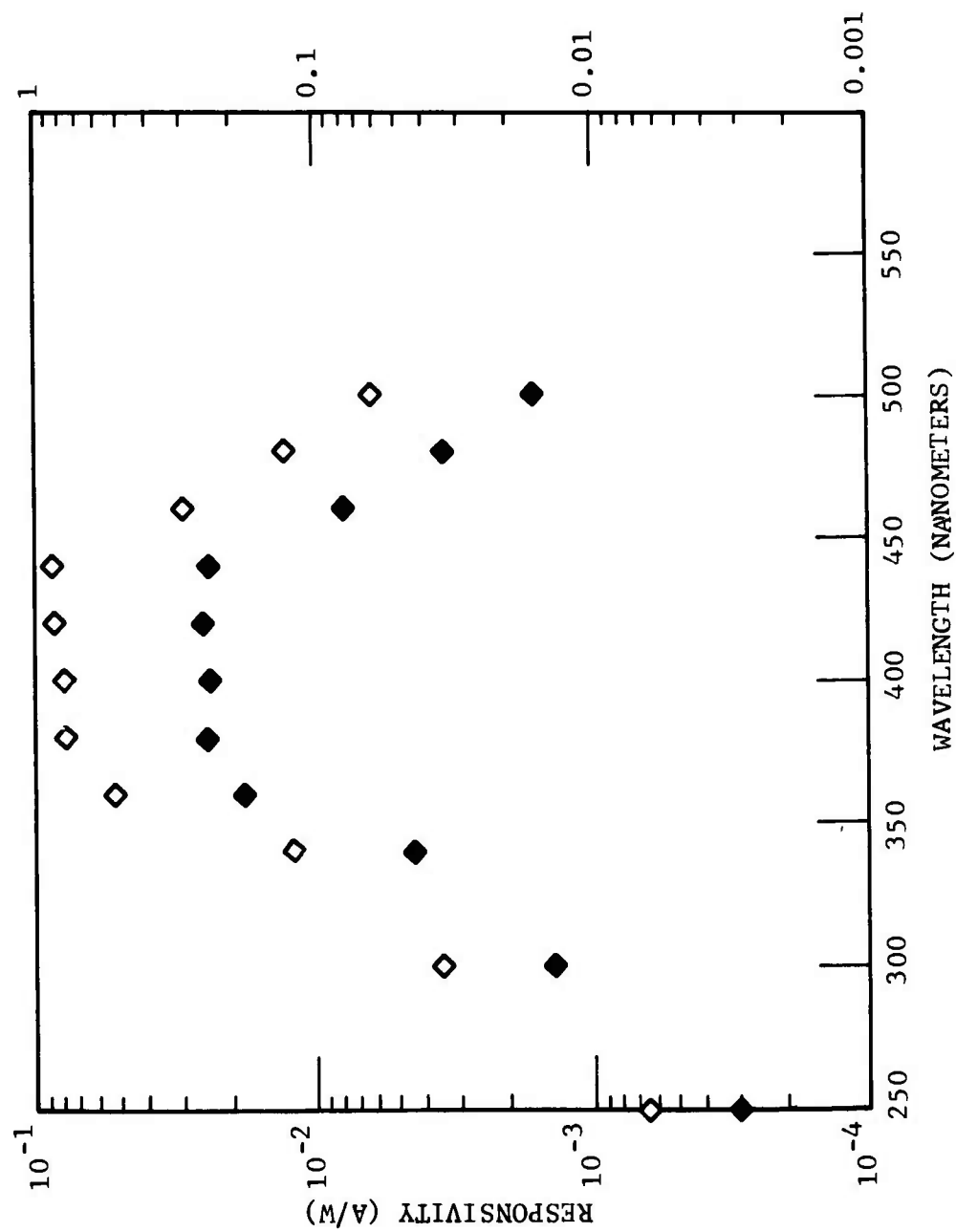
Figure 2 SPECTRAL RESPONSIVITY OF A TYPICAL DETECTOR AND QUANTUM
EFFICIENCY OF THAT DETECTOR VS WAVELENGTH
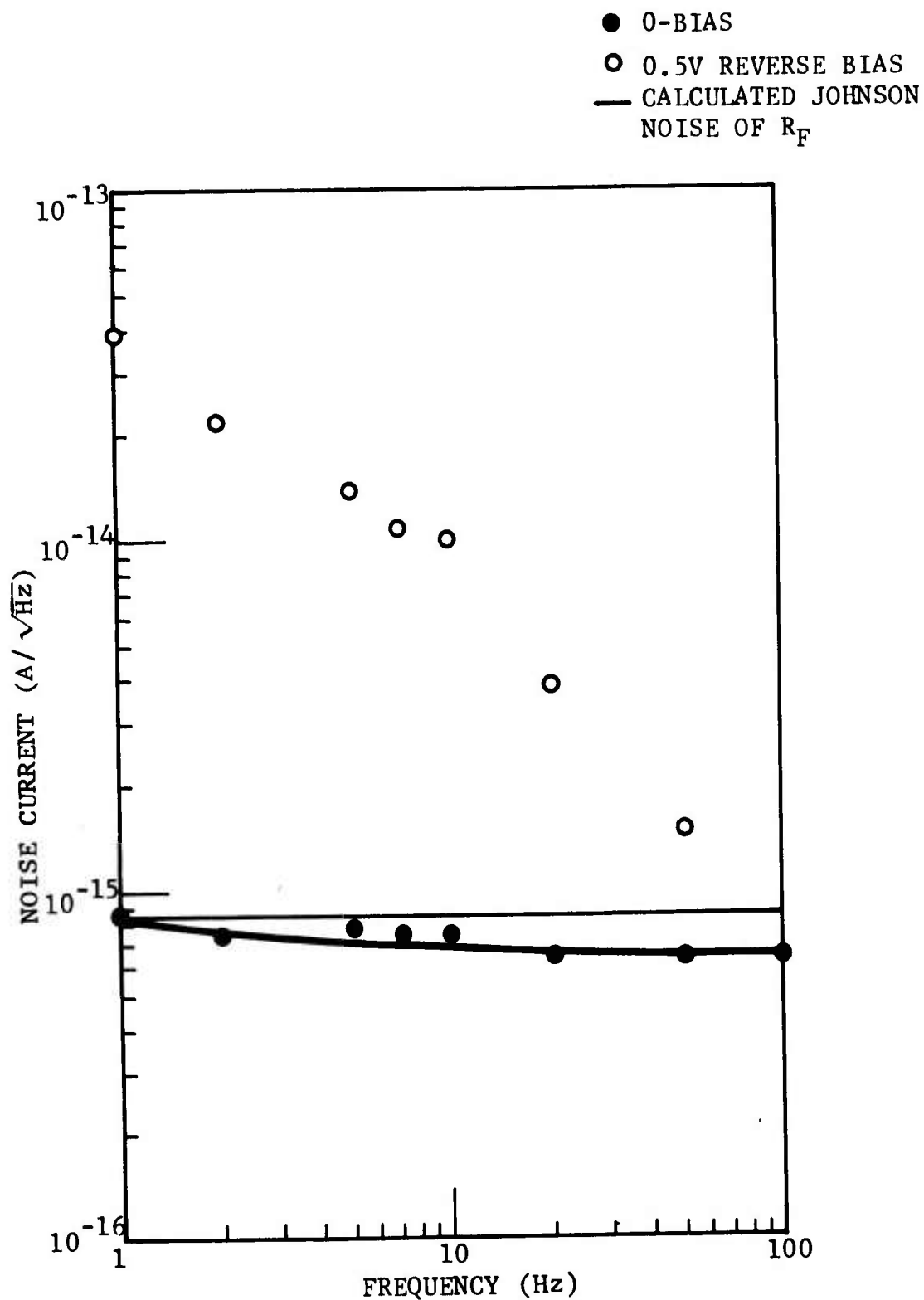
35

SECTION III

NOISE DATA
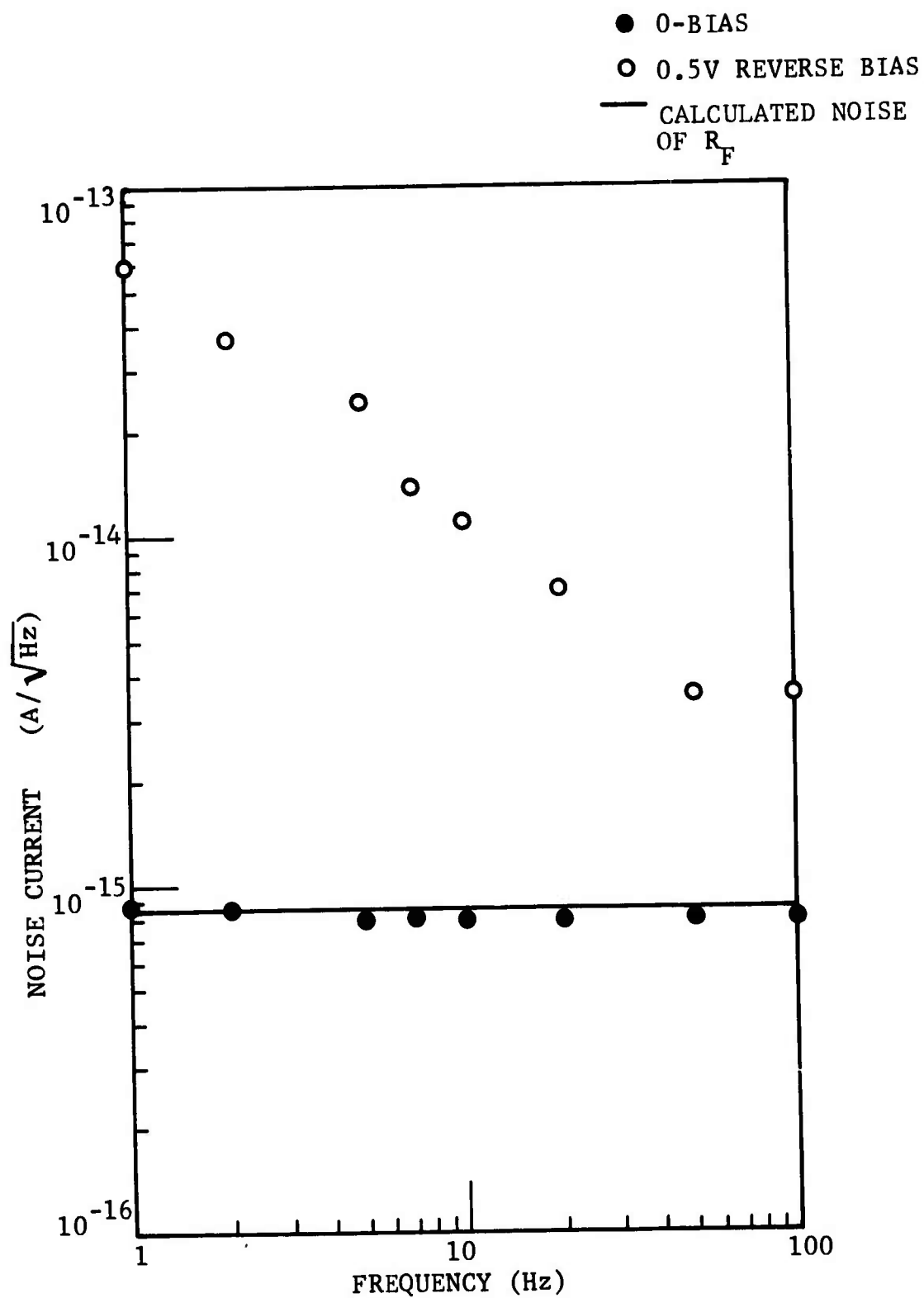
Figure 3 - Noise of Detector #1

Figure 4 - Noise of Detector #2

Figure 5 - Noise of Detector #3

Figure 6 - Noise of Detector #4

Figure 7 - Noise of Detector #5

NOTE: Noise of R_F is calculated Johnson's noise of 2.3×10^{10} Ω feedback resistor: 8.5×10^{-16} amps/$\sqrt{Hz}$

Figure 8 - Comparitive Detector NEPs

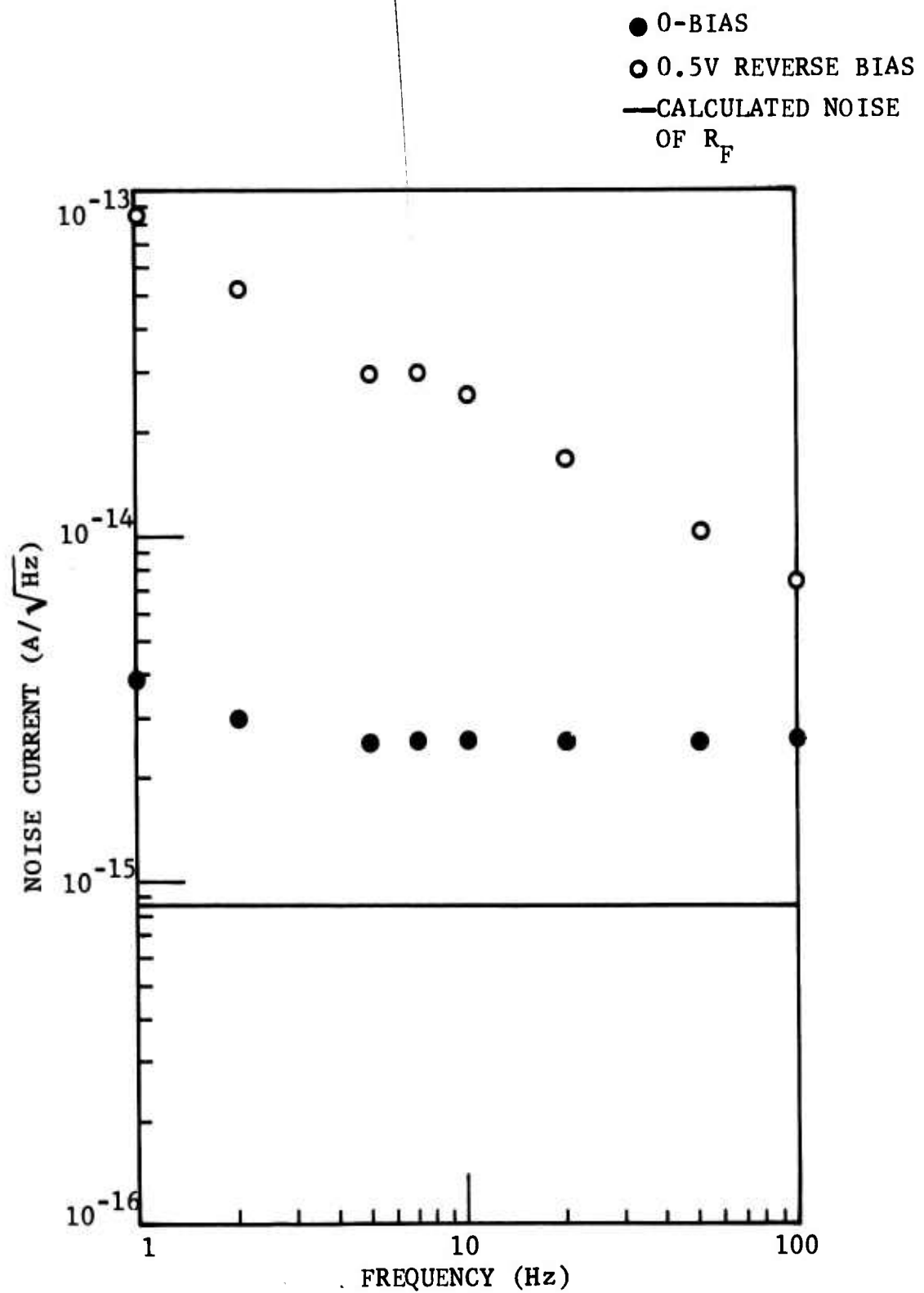Figure 3 NOISE OF DETECTOR #1

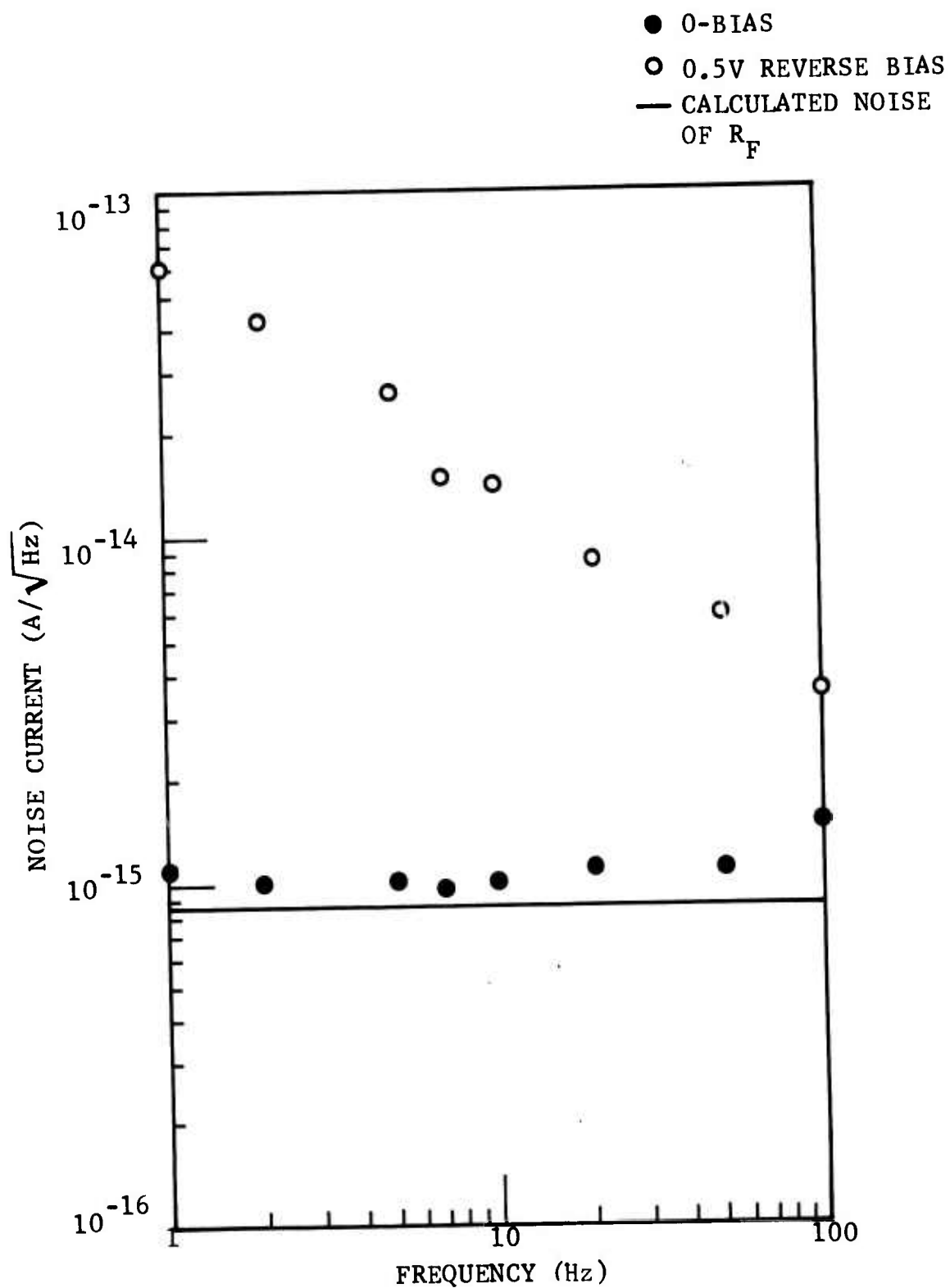Figure 4   NOISE OF DETECTOR #2

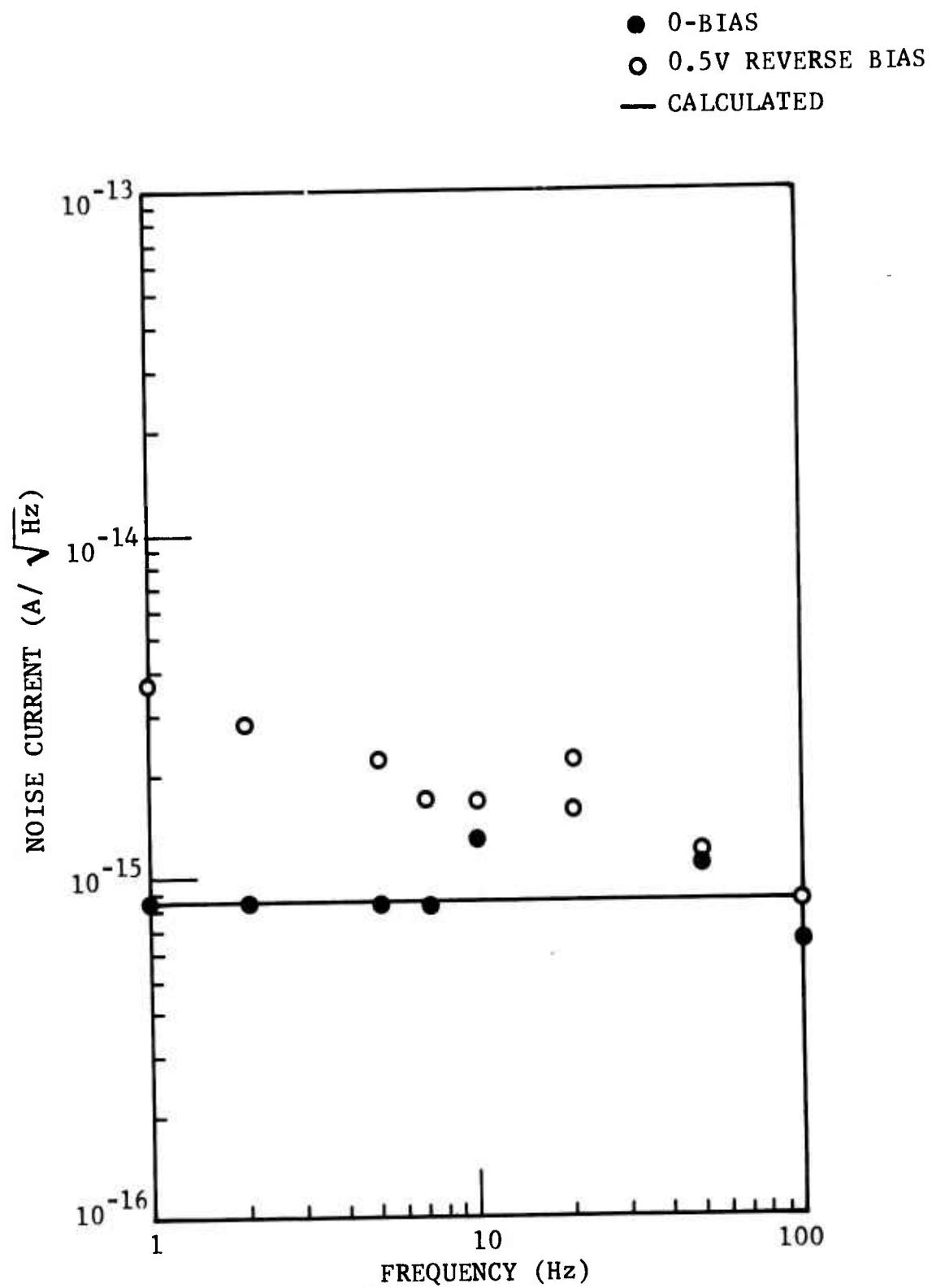Figure 5 NOISE OF DETECTOR #3

Figure 6 NOISE OF DETECTOR #4

40

Figure 7   NOISE OF DETECTOR #2
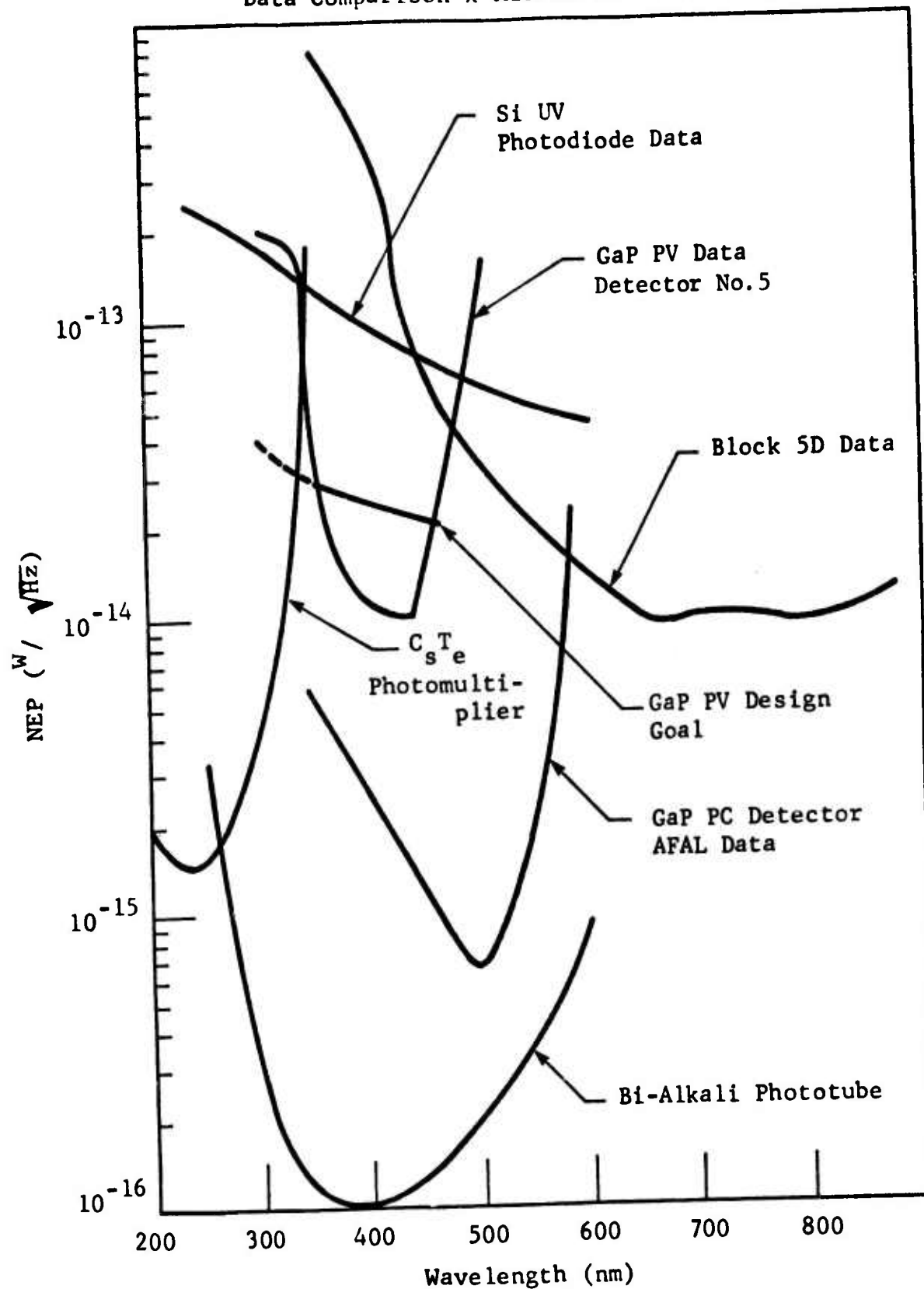
41

Data Comparison λ Alternative Detectors

Figure 8   COMPARATIVE DETECTOR NEPS

THIS REPORT HAS BEEN DELIMITED
AND CLEARED FOR PUBLIC RELEASE
UNDER DOD DIRECTIVE 5200.20 AND
NO RESTRICTIONS ARE IMPOSED UPON
ITS USE AND DISCLOSURE.

DISTRIBUTION STATEMENT A

APPROVED FOR PUBLIC RELEASE;
DISTRIBUTION UNLIMITED.